Available online at www.sciencedirect.com
ScienceDirect
Geochimica et Cosmochimica Acta 73 (2009) 3450–3470
Geochimica et Cosmochimica Acta
www.elsevier.com/locate/gca

Petrology, geochemistry, and age of low-Ti mare-basalt meteorite Northeast Africa 003-A: A possible member of the Apollo 15 mare basaltic suite

Jakub Haloda [a,b,*], Patricie Týcová [a,b], Randy L. Korotev [c], Vera A. Fernandes [d,e,1], Ray Burgess [d], Martin Thöni [f], Monika Jelenc [f], Petr Jakeš [b,2], Pavel Gabzdyl [g], Jan Košler [h]

[a] Department of Rock Geochemistry, Czech Geological Survey, 152 00 Prague, Czech Republic
[b] Institute of Geochemistry, Mineralogy and Mineral Resources, Faculty of Science, Charles University, 128 43 Prague, Czech Republic
[c] Department of Earth and Planetary Sciences, Washington University, C/B 1169, Saint Louis, MO 63130, USA
[d] School of Earth, Atmospheric and Environmental Sciences, University of Manchester, Manchester M13 9PL, UK
[e] Centro de Geofísica, Universidade de Coimbra, Coimbra 3000-134, Portugal
[f] Department of Lithosphere Research, University of Vienna, Althanstraße 14, A-1090 Vienna, Austria
[g] Department of Geological Sciences, Faculty of Science, Masaryk University, 611 37 Brno, Czech Republic
[h] Centre for Geobiology and Department of Earth Science, University of Bergen, Bergen N-5007, Norway

Received 5 November 2008; accepted in revised form 3 March 2009; available online 18 March 2009

Abstract

Northeast Africa 003 (NEA 003) is a lunar meteorite found as a two paired stones (6 and 118 g) in Libya, 2000 and 2001. The main portion (~75 vol%) of the 118 g meteorite, used for this study, (NEA 003-A) consists of mare-basalt and a smaller adjacent portion (~25 vol%) is a basaltic breccia (NEA 003-B). NEA 003-A has a coarse-grained magmatic texture consisting mainly of olivine, pyroxene and plagioclase. The late-stage mineral association is composed mainly of elongated plagioclase, ilmenite, troilite, fayalite, Si–K-rich glass, apatite, and a rare SiO_2 phase. Other accessory minerals include ulvöspinel, chromite, and trace Fe–Ni metal. Olivine and pyroxene contain shock-induced fractures, and plagioclase is completely converted into maskelynite.

The Fe/Mn values of the whole rock, olivines and pyroxenes, and the bulk-rock oxygen isotopic composition provide evidence for the lunar origin of NEA 003-A meteorite. This is further supported by the presence of Fe–Ni metal and the anhydrous mineral association.

NEA 003-A is geochemically and petrographically distinct from previously described mare-basalt meteorites and is not paired with any of them. The petrography and major element composition of NEA 003-A is similar to the composition of low-Ti olivine mare basalts from Apollo 12 and olivine-normative basalts from Apollo 15. The NEA 003-A meteorite shows obvious geochemical similarities in trace elements contents with Apollo 15 olivine-normative basalts and could represent a yet unknown geochemically primitive member of the olivine-normative basalt series. The meteorite is depleted in rare earth elements (REE) and incompatible trace elements indicating a primitive character of the parental magma. The bulk-rock chemical composition demonstrates that the parent melt of NEA 003-A was not contaminated with KREEP components as a result of magma mixing or assimilation processes. Results of crystallization modelling and low minimum cooling rate estimates (~0.07 °C/h) suggest that the parent melt of NEA 003-A crystallized in the lower part of a lava flow containing cumulate olivine (~10%) and was probably derived from more primitive picritic magma by fractional crystallization processes.

* Corresponding author. Address: Department of Rock Geochemistry, Czech Geological Survey, 152 00 Prague, Czech Republic.
E-mail address: jakub.haloda@geology.cz (J. Haloda).
[1] Present address: Berkeley Geochronology Center, Berkeley, CA, USA.
[2] Deceased 29 November 2005.

doi:10.1016/j.gca.2009.03.003

Sm–Nd dating yields an age of 3.09 ± 0.06 Ga which corresponds to the period of lower Eratosthenian lunar volcanic activity, and the near-chondritic ε_{Nd} value of -0.4 ± 0.3 indicates that the meteorite could be derived from a slightly enriched mantle source similar to the Apollo 15 green glasses. Ar–Ar step release results are inconsistent with Sm–Nd ages suggesting that NEA 003-A was exposed to one or more impact events. The most extensive event took place at 1.8 Ga and the shock intensity was likely between 28 and 45 GPa. The absence of solar Ar suggests that NEA 003-A has not been directly exposed at the lunar surface but the cosmic ray exposure age of 209 ± 6 Ma suggests that NEA 003-A resided in the upper regolith for part of its history.

1. INTRODUCTION

The current source of ground-truth information about the geology of the Moon is the approximately 382 kg of rock and regolith samples acquired by Apollo and Luna missions between 1969 and 1976. The Apollo and Luna rocks and regoliths sample the better characterized locations on the Moon, but these rocks are representative only of a small part of the lunar surface (about 16%; Korotev, 2005). Lunar meteorites originated from randomly distributed locations on the surface of the Moon and are likely to come from points distant from the Apollo sites (Korotev, 2005). Many of these meteorites have chemical and mineralogical features different from Apollo and Luna samples. From a total of more than 60 known lunar meteorites, only ten represent unbrecciated mare-basalt samples.

Northeast Africa 003 (NEA 003) is a lunar meteorite find composed of two stones. Both were found by a private collector 12 km NW from Al Qaryah Ash Sharqiyah in Wadi Zamzam area, Libya. The smaller of the two stones (6 g) was found in November 2000. The second stone (118 g) with incomplete fusion crust, which was used for this study, was found nearby in December 2001. All studied samples from this stone are deposited in Department of Rock Geochemistry of Czech Geological Survey. The meteorite contains two adjacent parts, mare-basalt and basaltic breccia. The main portion (~75 vol% of 118 g stone and ~55 vol% of 6 g stone) of the meteorite, designated NEA 003-A (Fig. 1), is an unbrecciated, coarse-grained, low-Ti olivine-rich mare-basalt. The remaining 25 and 45 vol%, respectively, of NEA 003-B, is a basaltic breccia consisting of well-consolidated glassy impact–melt matrix containing scattered mineral fragments with a chemical composition identical to the coarse-grained low-Ti olivine-rich basalt, and two larger clasts of different low-Ti mare-basalt lithologies (Haloda et al., 2006).

In this study we describe the main portion of NEA 003 lunar meteorite, the unbrecciated, low-Ti, olivine-rich mare-basalt designated NEA 003-A, and provide major- and trace-element compositional data along with Sm–Nd and Ar–Ar isotopic data. We show that this basalt is geochemically and petrographically distinct from the previously described mare-basalt meteorites and Apollo mare basalts (see Korotev (2005) for a review of all lunar meteorites known at that time) but that it could have a geological affinity to Apollo 15 olivine-normative basalts.

2. ANALYTICAL METHODS

2.1. Petrography, chemical composition and O isotope composition

Two polished thin sections (21×13 mm and 14×10 mm) and one polished thick section ($16 \times 20 \times 3$ mm) were prepared from different areas of NEA 003-A. Textural and mineralogical characteristics were studied using a LEICA DMLP petrographic microscope.

Backscattered electron (BSE) images and elemental X-ray maps were produced using a CAMSCAN 3200 scanning electron microscope fitted with an Oxford Instruments Energy Dispersive Spectral unit at the Czech Geological Survey in Prague, Czech Republic. Mineral modes were determined using the Area Measurement software (Oxford Instruments) and digital processing of BSE images and elemental X-ray maps.

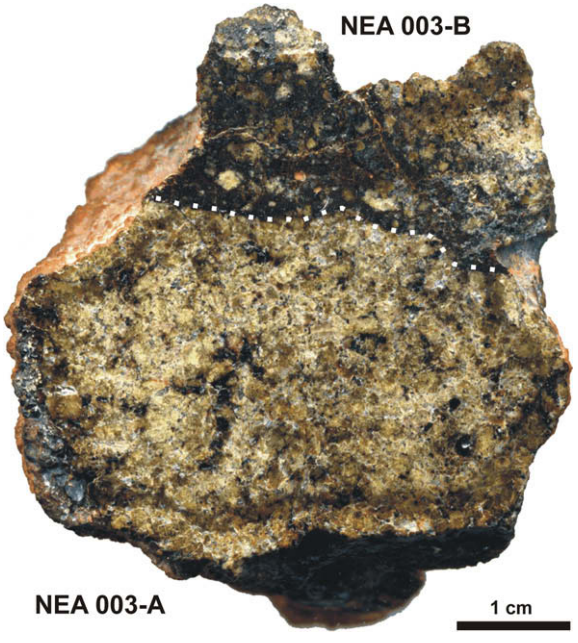

Fig. 1. Incident light image of a polished surface of Northeast Africa 003 lunar meteorite (118 g stone). The main part (~75 vol%) designated as NEA 003-A is an unbrecciated coarse-grained, low-Ti olivine-rich basalt. The adjacent part (NEA 003-B) is a basaltic breccia (~25 vol%).

Mineral compositions were determined using quantitative X-ray wavelength dispersive spectral analysis on an ARL SEMQ electron microprobe at the Naturhistorisches Museum, Vienna, Austria and a CAMECA SX100 electron microprobe at the Natural History Museum, London, UK. The analyses were performed using an accelerating voltage of 15 kV, 20 nA beam current, 1 μm beam size and ZAF correction procedures. The counting times were 20 or 30 s for all analyzed elements. To avoid Na volatilization during the analysis of glass and maskelynite, the beam size was increased to 5 μm. For both instruments a combination of natural and synthetic standards were used for calibration. Quantitative analysis obtained from these two instruments yielded consistent results.

The degree of maskelynitization of plagioclase, SiO_2 structure identification and crystallographic orientation of selected olivine grains were determined by electron backscattered diffraction (EBSD) methods (Schmidt and Olensen, 1989) using HKL Technology Nordlys-II system at Czech Geological Survey, Prague, Czech Republic.

The bulk-rock major and minor element concentrations were determined by XRF analyses. Analyses were performed using a wavelength-dispersive ARL 9400 ADVANT XRF system at Czech Geological Survey, Prague. A split of NEA 003-A with an original mass of 612.28 mg was cleaned in an ultrasonic bath and homogenized by crushing and powdering using an agate mortar and pestle. We analyzed three samples as pressed powder pellets, each sample was prepared from 150 mg of finely grounded sample powder. All XRF analyses were processed to determine measurement precision and average bulk element concentrations. The analytical errors (relative standard deviations) based on the average of 25 BHVO-1 reference standard measurements were better than 3% for Si, Ti, Al, Fe, Mg and Ca. For Cr and Mn the relative standard deviations were better than 7%.

The Na and K concentrations presented in this study were determined on a 50 mg aliquot from a 612.28 mg homogeneous powdered rock sample using ICP-OES. The sample was prepared following the method of Shafer et al. (2004). Analyses were performed using an Iris Advantage Thermo Jarrell Ash ICP-OES system at Czech Geological Survey, Prague. For ICP-OES system calibrations, we used certified reference materials BHVO-1 and BCR-2. Eight analyses were collected from this sample to determine measurement precision and the average element concentrations. The analytical errors (relative standard deviations) based on the average of 25 BHVO-1 reference standard measurements were better than 4% for both measured elements.

The concentration of trace elements including REEs of selected mineral grains from both thin and thick sections was determined using LA-ICP-MS analysis at University of Bergen, Norway. We used the Thermo Finnigan Element ICP-MS coupled to a New Wave UP-213 UV laser. The sample cell was flushed by He gas (99.9999% purity) which was mixed with Ar at the back end of the ICP torch before entering the plasma. The in situ analyses were carried out in a spot-mode, the laser beam of 25 μm diameter allowed us to obtain elemental concentrations of individual mineral grains. The external standards used were synthetic glasses NIST 610 and NIST 612. The relative standard deviations of _30 NIST 610 and 30 NIST 612 measurements were between 1% and 8% for the elements analyzed. Data were reduced using the Glitter software programme. Calcium was used as an internal standard by comparing the LA-ICP-MS CaO wt% abundance with the CaO wt% abundance measured by EMP.

The oxygen isotopic composition of NEA 003-A was determined at the Czech Geological Survey with the GEO 20-20 mass spectrometer using analytical procedures described by Clayton and Mayeda (1963, 1983).

Instrumental neutron activation analysis (INAA) was used to obtain compositional data for minor and trace elements in a 64-mg sample (chip) using the same techniques that have been used by Zeigler et al. (2005) for other lunar meteorites. These analyses were conducted at the Washington University in Saint Louis, USA.

2.2. Sm–Nd dating

Sieved fractions of NEA 003-A were prepared from the crushed bulk sample using conventional techniques. Mineral separates of plagioclase and pyroxene were handpicked in alcohol under a binocular microscope. The handpicked plagioclase (Pl) fraction was $\geqslant$99% pure, clinopyroxene fraction (Cpx) contained insignificant amount of olivine, partly as intergrowths. Impure fractions of plagioclase (Pl-impure), containing opaque phases and minor pyroxene intergrowths), and pyroxene (Cpx-impure), containing olivine and some maskelynite intergrowths, were also prepared. Furthermore, ~2 mg of distinctly black-brown clinopyroxene (Cpx–Fe-rich) grains were carefully handpicked to investigate the potential of within-grain Sm/Nd variation and, possible, age zonation, since clinopyroxene is strongly zoned with respect to major elements (see Section 3.2.2). The black-brown clinopyroxene fragments were identified using EMPA as being Fe-rich, and thus representing outer parts of large pyroxene grains.

Before dissolution the handpicked mineral fractions were rinsed repeatedly in acetone and deionised water in an ultrasonic bath. Sample splits for Sm–Nd analysis were washed for 30 min in warm (~70 °C) 0.8 N HCl to eliminate dust and surface contamination (terrestrial weathering and fluid infiltration, e.g. calcite).

Sample digestion for Sm–Nd isotope analysis was performed in screw-top Savillex® beakers using a mixture of ultrapure HF and $HClO_4$ (5:1 v/v) for 10 days at ~105 °C. After evaporation, the residues were treated with 5.8 N HCl several times. After each cooling, between 5 and 11% of the sample solution was decanted and spiked with a mixed Sm–Nd tracer (^{147}Sm–^{150}Nd) in order to determine Sm and Nd concentrations by isotope dilution (ID). The REE fraction was extracted using Bio-Rad AG® 50 W-X8 resin (200–400 mesh) and 4.0 N HCl. Neodymium and Sm were separated from the REE fraction in a Teflon-coated HdEHP column, and 0.18 N and 0.4 N HCl, respectively, as elution media. Maximum total procedural blanks were <50 pg for Sm and Nd, and thus taken as negligible.

A Finnigan® MAT262 mass spectrometer at the University of Vienna, Austria, was used for the analytical measurements in order to determine Sm and Nd concentrations. Samarium and Nd fractions for ID were loaded as nitrates and measured from Re double filaments. Measurements of Nd isotope compositions were run in static mode on a ThermoFinnigan® Triton TIMS instrument. A $^{143}Nd/^{144}Nd$ ratio of 0.511845 ± 0.000003 ($n = 7$, 2σ) was determined for the La Jolla (Nd) international standard during the period of this study. Within-run mass fractionation of Nd isotopes was corrected using $^{146}Nd/^{144}Nd = 0.7219$ (O'Nions et al., 1977). Uncertainties on the Nd isotope ratios are quoted as $2\sigma m$, uncertainties on the $^{147}Sm/^{144}Nd$ ratios are given as $\pm 1.0\%$, thought to represent maximum errors; the isochron regression calculation is based on these uncertainties. Age errors are given at the 2σ level. Isochron calculation follows Ludwig (2003). Ages are based on decay constants of $6.54 \times 10^{-12}\ y^{-1}$ for ^{147}Sm (Lugmair and Marti, 1978); ε_{Nd} is calculated following the chondritic uniform reservoir (CHUR) parameters of Hamilton et al. (1983).

2.3. Ar–Ar dating

Bulk samples of NEA 003-A were analyzed using both furnace and laser step heating techniques at the University of Manchester. Mineral separates of predominantly pyroxene and predominantly maskelynite were hand-picked from bulk samples after irradiation and step heated using an infra-red (IR)-laser with the aim of further understanding the features observed in age spectra obtained from bulk samples. A total of 23.60 mg of NEA 003-A was positioned between Hb3gr monitors (1072 ± 11 Ma; Turner, 1971) in a silica glass vial and irradiated with a fast neutron fluence of 1.67×10^{18} neutrons cm^{-2}. The irradiation was carried-out in position B2W of the SAFARI-1 reactor at Pelindaba, South Africa. During stepped heating in a resistance furnace, Ar gas was released over the temperature interval of 300–1600 °C using steps of 100 °C or 50 °C and 30 min duration. Argon isotopes were measured using the MS1 mass spectrometer equipped with a Baur-Signer ion source and single Faraday and electron multiplier channeltron detectors. The furnace blank at low temperatures (400–1100 °C) is equivalent to $753 \pm 2 \times 10^{-12}\ cm^3$ STP ^{40}Ar which increases at high temperature (⩾1300 °C) to $3547 \pm 6 \times 10^{-12}\ cm^3$ STP ^{40}Ar. The furnace blanks have an approximately atmospheric Ar isotope composition.

The IR-laser probe employs Nd-YAG continuous wave laser ($\lambda = 1064$ nm). Typical blank is equivalent to $25.7 \pm 0.5 \times 10^{-12}\ cm^3$ STP ^{40}Ar. Argon was extracted using between 13 and 24 heating steps each 1 min duration, with a defocused beam of 3 mm diameter and a maximum of 15 W laser output power. The temperature was controlled by increasing the flashlamp current within the laser output range 2–5 W and analyses continued until the sample was fused. Data for both furnace and IR laser stepped heating have been corrected for blanks, mass discrimination and neutron interference isotopes. Errors on Ar–Ar step ages includes the 1% difference in J value ($J = 0.008808 \pm 0.00013$, including monitor age error) obtained for the monitors and, for total ages, an additional 1.4% uncertainty introduced by the error on the age determination of the Hb3gr monitor. The decay constant value used is $5.543 \times 10^{-10}\ y^{-1}$ (Steiger and Jäger, 1977). Ar–Ar ages are reported at the two standard deviation (2σ) level of uncertainty. Further details of the experimental methods and data reduction procedures are given in Fernandes et al. (2000) and Fernandes and Burgess (2005).

3. RESULTS

3.1. Oxygen isotope composition and confirmation of lunar origin

Several lines of evidence support a lunar origin of NEA 003-A. Fe/Mn atomic ratios of the whole rock (81), olivines (93–110) and pyroxenes (43–89) of NEA 003-A (Haloda et al., 2006) are typical of lunar basalts and distinct from those of other meteorites (Papike et al., 2003). The NEA 003-A bulk-rock oxygen isotope composition of $\delta^{18}O = 5.76 \pm 0.08‰$ (1σ) and $\delta^{17}O = 3.04 \pm 0.05‰$ (1σ) lies on the terrestrial fractionation line (Fig. 2), which is characteristic for lunar rocks (Spicuzza et al., 2007 and references therein) and corresponds to the range of Apollo 12 and Apollo 15 basalts. Additional evidence for the lunar origin of NEA 003-A is the presence of Fe–Ni metal and absence

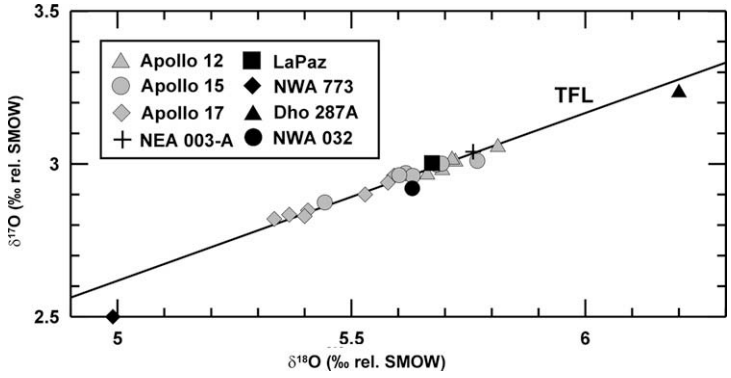

Fig. 2. Oxygen isotopic composition of NEA 003-A plots along the terrestrial fractionation line (TFL) with other basaltic lunar meteorites and Apollo 12, Apollo 15 and Apollo 17 samples. Data sources: NEA 003-A (this study), other lunar samples (Spicuzza et al., 2007).

of water-bearing minerals, which together are indicative of petrogenesis within oxygen fugacities lower than for terrestrial basalts but prevalent in lunar magmatic systems.

3.2. Petrography, textures and mineral chemistry

NEA 003-A has a coarse-grained porphyritic magmatic texture consisting mainly of olivine, pyroxene and plagioclase grains (Fig. 3). Accessory minerals in NEA 003-A include ilmenite, ulvöspinel, chromite, troilite and trace Fe–Ni metal. The distribution of silicate minerals in NEA 003-A is relatively homogeneous. Only small parts of the sample are represented by the late-stage mineral association composed mainly of elongated plagioclase, ilmenite, troilite, fayalite, a rare SiO_2 phase, chlorapatite and Si–K-rich glass (Fig. 3e and f). Other minerals, such as K–Ba-rich glass, K-feldspar, fluorapatite, and REE-merrillite (Jolliff et al., 2006) that are commonly associated with mesostasis in other lunar basalts (Papike et al., 1998) were not found in this sample. Olivine, pyroxene and spinel grains have numerous cracks and fractures that are probably due to shock effects (see Fig. 3). Some of the larger near-surface fractures of the meteorite are filled with the products of terrestrial weathering (mainly secondary Ca-carbonate). Shock event(s) resulted in conversion of all plagioclase into maskelynite. Thin veinlets of melt are present along mineral grain boundaries due to shock metamorphism.

With respect to modal mineralogy, NEA 003-A is most similar to Apollo 12 and Apollo 15 basalts (Table 1). In the following sections, we describe the detailed characteristics of individual minerals and their inter-relationships.

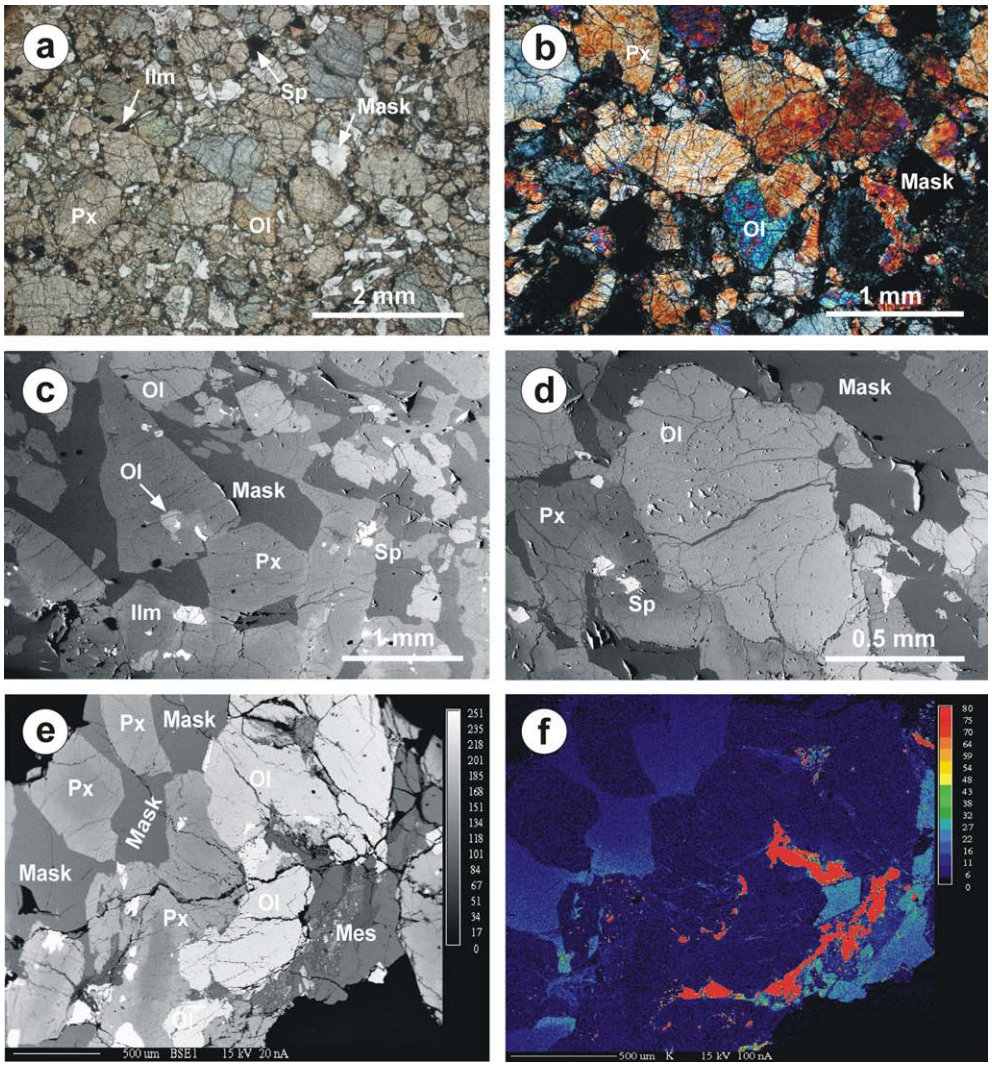

Fig. 3. Photomicrographs, BSE images and element map illustrating the textures and mineralogy of NEA 003-A: (a) coarse-grained olivine-rich low-Ti basalt with typical magmatic texture in plane polarised light; (b) the detail of previous image in polarised light (crossed nicols); (c) BSE image of a part of NEA 003-A lunar meteorite with porphyritic texture, note the olivine grain partially replaced by pigeonitic pyroxene; (d) detailed BSE view of the olivine grain (Ol, olivine; Px, pyroxene; Mask, maskelynite; Sp, spinel; Ilm, ilmenite); (e) BSE image of the porphyritic texture of NEA 003-A with mesostasis region (Mes); and (f) element distribution X-ray map for K showing the K-rich glass in the mesostasis.

Table 1
Modal abundances (vol%) of selected mare-basalt meteorites and similar basalts from Apollo 12 and Apollo 15.

	Mare-basalt meteorites						Apollo 12 and Apollo 15 basalts		
	NEA 003-A	LAP 02205	Dho 287A	NWA 032	Y-793169	A-881757	12040	12012	15555,8
Olivine phenocrysts	17.5	1.2	20.6	11.3	0.0	0.0	22.7	21.6	6.9
Chromite phenocrysts	0.5	0.1	0.4	0.3	0.0	<5	1.2	0.7	0.1
Undifferentiated pyroxene	60.6	56.9	47.4	50.7	56.0	59.0	51.5	53.5	66.8
Feldspar/maskelynite	18.2	33.1	25.9	29.4	42.0	30.0	21.6	19.0	19.7
Silica	tr	2.3	0.2	0.0	0.0	0.0	0.1	0.2	tr
Ulvöspinel	0.3	0.4	0.8	tr	1.0	<5	0.0	0.6	0.4
Ilmenite	1.2	3.3	2.3	4.4	1.0	6.0	2.3	1.9	5.6
Troilite	tr	0.2	0.1	0.7	0.0	<5	0.2	0.4	tr
Fe–Ni metal	tr	tr	tr	tr	0.0	<5	0.0	0.5	tr
Opaque minerals (total)	2.0	4.0	3.6	5.4	2.0	<11	3.7	4.1	6.1
Phosphate	tr	0.3	0.6	—	—	—	—	—	—
Fayalite	tr	1.5	0.2	—	—	—	—	—	—
Shock-melt glass	1.5	0.8	1.4	3.2	0.0	0.0	—	—	—
Volcanic glass/mesostasis	0.2	>4	>3	0.0	0.0	0.0	0.3	1.9	0.3

Data sources: NEA 003-A (this study), LAP 02205 (Anand et al., 2006), Dhofar 287A (Anand et al., 2003), NWA 032 (Fagan et al., 2002), Y-793169 (Takeda et al., 1993), A-881757 (Yanai and Kojima 1991), Apollo 12 basalts: 12,040 and 12,012 (Neal et al., 1994), Apollo 15 basalts: 15555,8 (Rhodes and Hubbard, 1973).

3.2.1. Olivine

Olivines in NEA 003-A are characterized by a great number of euhedral and subhedral grains (0.2–1.4 mm, typically >0.6 mm) with elongate to equant shapes and chemical zonation. The majority of olivines show normal symmetrical zoning with Mg-rich cores and Fe-rich rims, but there are also several olivine grains that show asymmetrical zoning with gradual iron enrichment along their edges. This observation can be best explained by the early-formed olivines being only partially in contact with Fe-enriched melt during crystallization. The early-formed olivine grains often have circular or rounded inclusions of chromite or recrystallized melt-inclusions consisting of fine-grained pyroxene and feldspar. A significant number of Mg-rich olivine ($Fo > 58$) grains are completely enclosed in pigeonitic pyroxene (Fig. 3c). This textural feature is indicative of a reaction between Mg-rich olivines and pyroxenes, where enclosed olivines were partially replaced by pigeonitic pyroxene formed by the reaction olivine + liquid → pigeonite.

Mosaic extinction of olivine grains indicates a deformation of crystal structure and the presence of numerous cracks and fractures suggests an intensive shock process. Based on the barometric classification of Stöffler and Grieve (2007) for basaltic rocks, the shock pressures undergone by this rock are estimated between 28 and 45 GPa (shock stage 2b).

Electron microprobe data for 305 olivine spot analyses were collected to obtain the representative range of Fo components (Fig. 4a and Table 2). CaO concentrations vary from 0.1 to 0.6 wt%, TiO_2 is <0.2 wt%, the Cr_2O_3 range is 0.05–0.5 wt% and the MnO range is 0.2–0.6 wt%. Distribution of the Fo component (in the majority of olivine grains) is in range of $Fo_{73\text{-}19}$ with a mode at about Fo_{53}. The lower frequency in the range of $\sim Fo_{73\text{-}60}$ reflects the partial replacement of Mg-rich olivine by pigeonite. The range of olivine composition is comparable with other mare-basalt meteorites and mare-basalts from Apollo 12 (olivine, pigeonite and ilmenite basalts) and Apollo 15 (olivine-normative basalts), (Fig. 4b). However, the fayalitic olivine typical of mesostasis mineral associations, which has been described for many mare-basalts (e.g. Dhofar 287A, LAP 02205; Basaltic Volcanism Study Project, 1981; Anand et al., 2003; Day et al., 2006) is rare in NEA 003-A (Fig. 4a) because of the lack of mesostasis-rich areas. Variation of the Fo component within several olivine grains was also investigated by collecting electron microprobe data along two orthogonal profiles in each grain (see Section 3.4. for more discussion).

3.2.2. Pyroxenes

Pyroxene is the most abundant phase in NEA 003-A occurring mainly as subhedral grains (0.5–1 mm) and showing similar petrographic features (e.g. shock related) to large olivine crystals (Fig. 3a–e). The grains are generally equant to slightly elongated and are characterized by mosaic extinction and symmetrical chemical zonation. Pyroxenes often contain inclusions of olivine, chromite and ulvöspinel.

The chemical composition of pyroxene shows extreme variations in terms of Mg–Fe–Ca contents following a typical mare-basalt fractionation trend (Fig. 5a). Characteristic zoning of pyroxene is represented by Mg-enriched cores ($En_{69\text{-}47}$, $Wo_{7\text{-}33}$), Ca-Fe-enriched mantles ($En_{55\text{-}40}$, $Wo_{15\text{-}38}$) and Fe-enriched rims ($En_{45\text{-}2}$, $Wo_{35\text{-}12}$). The core-to-mantle Ca-enrichment of pyroxene grains is usually not continuous. This feature reflects a discontinuity in the chemical composition between Mg-rich pigeonite and Ca-rich augite (Fig. 5a). Only a few pyroxene grains at the contact with late-stage minerals show gradual Fe enrichments in their rims towards pyroxferroite composition. Representative compositions of the main types of pyroxene are listed in Table 2.

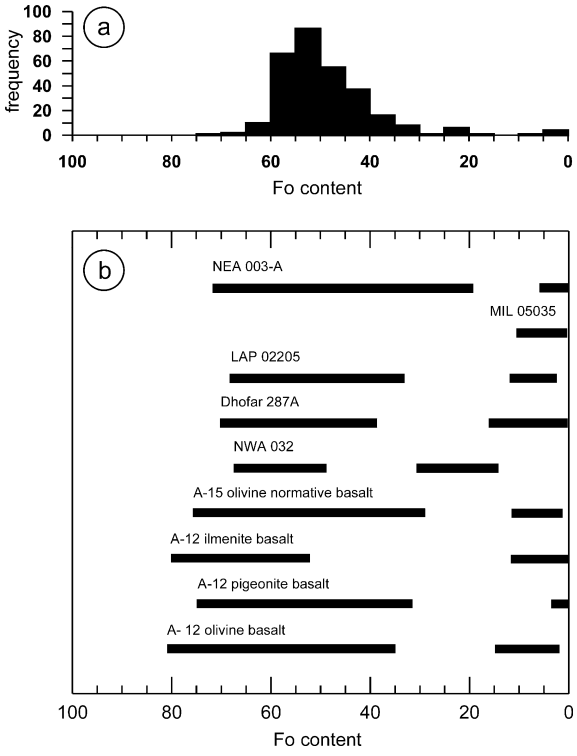

Fig. 4. Composition of olivines in NEA 003-A. (a) A histogram of Fo content in olivine. (b) Comparison of olivine Fo content of NEA 003-A with other selected mare-basalt meteorites and Apollo 12 and Apollo 15 samples. *Data sources:* MIL 05035 (Joy et al., 2008), LAP 02205 (Anand et al., 2006), Dhofar 287A (Anand et al., 2003), NWA 032 (Fagan et al., 2002), Apollo 12 and Apollo 15 basalts (Basaltic Volcanism Study Project, 1981).

Mg-rich cores of pyroxene grains are relatively depleted in high field-strength elements with $\Sigma(Al, Ti, Cr) \approx 0.08$ atoms per formula unit (based on 6-oxygen) in contrast with enrichment in the mantle $\Sigma(Al, Ti, Cr) \approx 0.15$ and in the rim $\Sigma(Al, Ti, Cr) \approx 0.11$ of the grains. The Ti/Al ratios in pyroxene vary depending upon appearance of other liquidus phases during magma crystallization. Aluminium in the cores and mantles of pyroxene enters the pyroxene crystal structure both by Tschermak substitution ($AlAlMg_{-1}Si_{-1}$) and coupled titanian ($TiAl_2Mg_{-1}Si_{-2}$) exchange reactions (Thompson, 1982). The Ti/Al ratios in Mg-rich pyroxene cores vary from 0.25 to 0.3 and reflect initial pigeonite crystallization (Fig. 5b). Ca–Fe-rich pyroxene mantles have typically higher concentrations of Al and Ti due to accommodation of larger amounts of these elements in Ca-rich pyroxene during crystallization compared to Mg-rich pyroxene. However, the initial Ti/Al values (0.25–0.3) sharply increase to 0.5. This change in Ti/Al can be interpreted as being due to the appearance of plagioclase on the liquidus, when the amount of Al uptake into the pyroxene structure was affected by plagioclase crystallization (Fig. 5b). Fe-rich pyroxene rims usually have lower concentration of Al and Ti compared to Ca–Fe-rich pyroxene mantle. The decrease of Ti concentration relates to appearance of ilmenite on the liquidus. Crystallization of ilmenite together with plagioclase and pyroxene leads to the titanium depletion of the residual magma. The Ti/Al values of Fe-rich pyroxene rims vary usually from 0.5 to 0.75. Ti/Al can be close to 1.0 for pyroxene rims with strong Fe-enrichment where they are in contact with late-stage minerals. Small differences in Ti/Al for Fe-rich pyroxene rims indicate that pyroxene, plagioclase and ilmenite crystallized at the same time. The crystallization sequence of major mineral phases of NEA 003-A, derived from variations of Ti and Al contents in pyroxene, is in good agreement with results of crystallization modelling (see Section 3.4). Concentrations of Ti and Al (atoms per 6-oxygen formula unit) of pyroxene cores, mantles and rims, together with a representative profile across one selected pyroxene grain, are shown in Fig. 5b.

3.2.3. Plagioclase feldspar

Plagioclase feldspar of NEA 003-A has the lowest modal abundance (18.2%; Table 1) among all known low-Ti mare-basalt meteorites. The absence of diffraction patterns confirmed by the EBSD method suggests that plagioclase was completely converted into diaplectic glass (maskelynite) during a shock event(s) associated with the impact processes. Total conversion of plagioclase to maskelynite proceeds at a pressure of about 28–45 GPa with a post-shock temperature increase of 200–250 °C (Stöffler and Grieve, 2007). From the total of 10 unbrecciated mare-basalt meteorites only NEA 003-A, Dhofar 287-A (Anand et al., 2003) and Asuka 881757 (Yanai et al., 1993) are showing complete plagioclase to maskelynite conversion. The maskelynite has generally irregular shapes and occasionally occurs as slightly elongate grains (see Fig. 3). Maskelynite compositions fall within the range $An_{84\text{-}92}$, which is typical for the majority of mare-basalts from Apollo 12 and Apollo 15 (Basaltic Volcanism Study Project, 1981; Papike et al., 1998).

3.2.4. Accessory minerals

Accessory minerals of NEA 003-A comprise ilmenite, spinels, Fe–Ni metal, troilite and rare fayalite, Si–K-rich glass, SiO_2 phase and apatite.

Ilmenite is the most abundant opaque phase in this meteorite and forms lath-shaped grains (typically 50–200 μm long) often associated with ulvöspinel. Textures indicating typical subsolidus reduction of ulvöspinel to ilmenite and Fe metal are rarely present (El Goresy, 1976).

Spinel in NEA 003-A occurs as chromite and ulvöspinel. Chromite forms euhedral crystals typically 50–100 μm across, surrounded by other minerals, and is often enclosed in olivine and occasionally in pyroxene. The chemical composition of chromite is near to the chromite end-member of spinel solid solution, with low concentrations of TiO_2, MgO and Al_2O_3 (Table 2 and Fig. 6). Grains composed of a chromite core and rimmed by ulvöspinel are common, occurring mainly at ilmenite–pyroxene–plagioclase grain boundaries. Ulvöspinel rims around chromite were not observed in the case of chromite inclusions within olivine or pyroxene. The boundaries between chromite and ulvöspinel are sharp. The microprobe data for NEA 003-A spinels show a typical fractionation trend (Fig. 6a and b) similar to those observed in A-12 and A-15 basalts (El Goresy et al. 1971; Taylor et al., 1971; El Goresy, 1976).

Table 2
Representative electron microprobe analyses (wt%) of minerals and shock melt glass of NEA 003-A.

Phase	Olivine (core)	Olivine (rim)	Mg-rich pyroxene (core)	Mg–Ca-rich (mantle)	Fe-rich pyroxene (rim)	Fe–pyroxene	Chromite	Ulvöspinel	Ilmenite	Maskelynite	Cl-apatite	Si–K-rich glass
SiO_2	36.84	31.35	52.62	50.80	48.62	44.60	nd	nd	bd	45.67	nd	76.10
TiO_2	0.06	0.07	0.50	1.01	1.27	0.52	6.26	28.93	53.06	nd	nd	0.56
Al_2O_3	0.08	0.11	1.18	2.70	1.57	0.59	11.14	3.06	0.05	33.85	nd	12.80
Cr_2O_3	0.09	0.05	0.68	0.94	0.30	0.04	44.71	10.26	bd	nd	nd	nd
MgO	33.33	9.22	22.81	16.04	9.85	0.04	4.04	1.55	0.29	bd	0.09	0.32
CaO	0.34	0.48	4.50	16.37	15.67	5.00	0.16	0.02	0.17	18.90	52.47	0.45
MnO	0.30	0.53	0.29	0.21	0.34	0.54	0.35	0.43	0.26	nd	nd	0.04
FeO	28.99	58.06	16.90	12.31	22.18	47.94	32.97	55.58	45.51	0.55	1.21	0.62
Na_2O	nd	nd	0.02	0.05	0.05	0.07	nd	nd	nd	0.95	bd	0.67
K_2O	nd	nd	0.003*	0.005*	0.009*	0.010*	nd	nd	nd	0.07	nd	8.67
NiO	bd	bd	bd	bd	0.02	bd	bd	bd	bd	nd	nd	nd
P_2O_5	nd	nd	nd	nd	nd	nd	nd	nd	nd	nd	40.95	nd
Cl	nd	nd	nd	nd	nd	nd	nd	nd	nd	nd	2.94	nd
F	nd	nd	nd	nd	nd	nd	nd	nd	nd	nd	0.68	nd
Total	100.03	99.87	99.49	100.43	99.92	99.26	99.63	99.83	99.34	99.99	98.34	100.23
Oxygen basis	4	4	6	6	6	6	4	4	3	8	24	
Si	0.991	0.991	1.945	1.890	1.907	1.951	—	—	—	2.114	—	—
Ti	0.001	0.002	0.014	0.028	0.037	0.017	0.161	0.789	1.009	—	—	—
Al	0.002	0.004	0.051	0.119	0.073	0.030	0.450	0.131	0.002	1.847	—	—
Cr	0.002	0.001	0.020	0.028	0.009	0.001	1.211	0.294	—	—	—	—
Mg	1.336	0.434	1.257	0.890	0.576	0.002	0.206	0.084	0.011	—	0.014	—
Ca	0.010	0.016	0.178	0.653	0.659	0.234	0.006	0.001	0.005	0.938	9.979	—
Mn	0.007	0.014	0.009	0.007	0.011	0.020	0.010	0.013	0.006	—	—	—
Fe	0.652	1.534	0.522	0.383	0.728	1.753	0.944	1.687	0.962	0.021	0.250	—
Na	—	—	0.001	0.004	0.009	0.001	—	—	—	0.080	—	—
K	—	—	—	—	—	—	—	—	—	0.005	—	—
Ni	—	—	—	—	0.001	—	—	—	—	—	—	—
P											4.756	
Total	3.001	2.996	3.997	4.002	4.010	4.009	2.988	2.999	1.995	5.005	15.000	—
Mg#	67.0	22.1	69.3	69.9	44.2	0.0	—	—	—	—	—	—
Fe/Mn (atom.%)	94.8	107.5	50.1	57.6	66.2	87.7	—	—	—	—	—	—

Nd, not determined; bd, below detection; Fe-pyroxene, pyroxferroite.
* Pyroxene K_2O concentrations were calculated from LA-ICP-MS analyses.

Fe–Ni metal grains are rare, with Ni and Co concentrations in the range of 3–39 and 0.1–1.6 wt%, respectively. Troilite occurs in the form of irregular grains and together with Fe–Ni metal is adjacent to late-stage mineral associations.

A distinctive petrographic feature of NEA 003-A is the low amount of late-stage mesostasis (<0.2 vol%) when compared to other mare basalts. The late-stage mineral association can be found in several interstitial residual melt pockets between the mafic silicate grains and is composed of elongated plagioclase, ilmenite, troilite, fayalite, Si–K-rich glass, a rare SiO_2 phase (which was identified as a glass by EBSD) and apatite (Figs. 3e and f and 7). The typical mesostasis "Swiss-cheese" texture found in Dho 287A and LaPaz Icefield 02205 (Anand et al., 2003, 2006; Day et al., 2006) is not present in NEA 003-A due to low content of these immiscible residual melts.

Shock veins and melt pockets are widely dispersed in the sample, containing small mineral fragments and bubbles. They consist of shock-melted glass with basaltic composition very similar to the composition of the whole-rock meteorite (Table 2).

3.3. Whole-rock chemical composition

The whole-rock major and trace element compositions of NEA 003-A and other similar mare basalts are listed in Table 3. Based on the classification of Neal and Taylor (1992) and the mineral composition of the meteorite, NEA 003-A can be classified as low-Ti, low-Al, low-K, olivine-rich basalt similar to olivine basalts from Apollo 12 and olivine-normative basalts from Apollo 15. The relationship between Al_2O_3 and MgO in NEA 003-A (Fig. 8b) is also consistent with the trend of olivine crystallization in olivine basalts from both Apollo 12 and Apollo 15 (Papike et al., 1998). The TiO_2 to MgO (Fig. 8c) ratio in NEA 003-A is lower than the values observed in Apollo 12 samples, but consistent with Apollo 15 trend. There is a minor difference in the FeO content of NEA 003-A obtained using two different analytical methods: INAA FeO = 18.5–20.1 wt% for

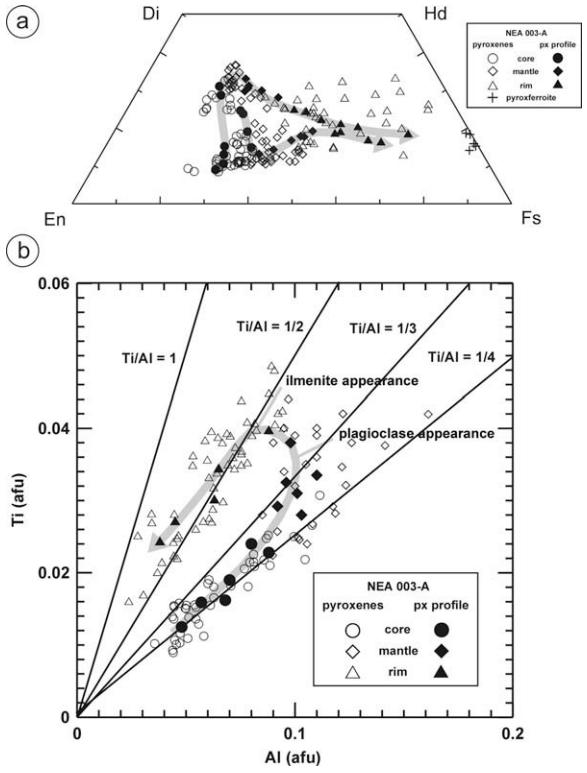

Fig. 5. (a) Pyroxene composition plot for NEA 003-A pyroxenes, two profiles across pyroxene grains (full symbols) show typical trend of composition change during crystallization. (b) Concentration of Al and Ti (atoms per 6-oxygen formula unit) for NEA 003-A pyroxene cores, mantles and rims. The profile across the pyroxene grain (full symbols) show the changes in Al and Ti content during crystallization.

three subsamples, mean value = 19.3 wt%; and XRF FeO = 21.8 wt%. This discrepancy can be explained by the coarse grain size of the meteorite combined with the large difference in sample masses used for analysis (64 mg INAA and 450 mg XRF).

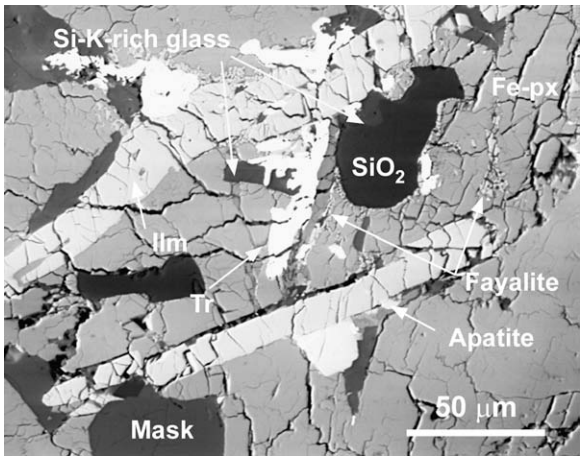

Fig. 7. BSE image of mesostasis area of NEA 003-A with typical late-stage mineral association (Fe–px, Fe-rich pyroxene; Mask, maskelynite; Tr, troilite; Ilm, ilmenite).

The high Co concentration compared to other similar mare basalts (Table 3.) and high Co/Sc ratio reflects the high modal proportions of olivine in the rock. The REE concentrations in NEA 003-A (Table 3 and Figs. 9b–d and 10) are at the low end of the range for Apollo 12 and Apollo 15 basalts. The chondrite-normalized REE pattern of NEA 003-A is flat with small but resolvable Eu depletion a feature typical of many mare basalts (Fig. 10). The low absolute concentration of Eu (0.60 ppm; Table 3) reflects the low modal abundance of plagioclase.

3.4. Crystallization modelling

In order to calculate the Fo content of olivine in equilibrium with a whole rock Mg# (Roeder and Emslie, 1970; Langmuir and Hanson, 1981), we used TiO_2 calibrated K_d (distribution coefficient relating the partitioning of iron and magnesium between olivine and a co-existing low-Ti

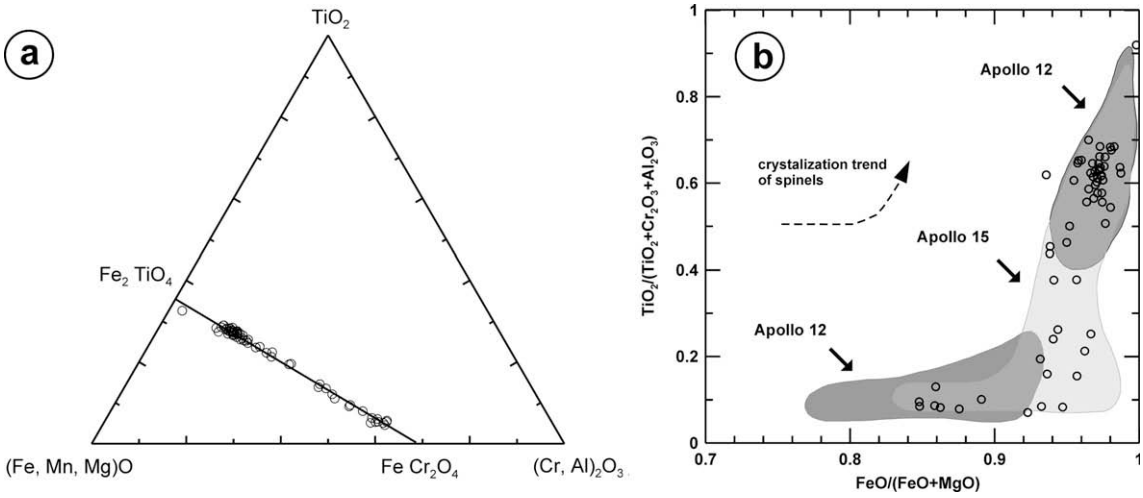

Fig. 6. Composition of spinels from NEA 003-A. (a) Ternary plot (in wt%) after El Goresy (1971) for NEA 003-A spinel composition. (b) FeO/(FeO + MgO) vs. $TiO_2/(TiO_2 + Cr_2O_3 + Al_2O_3)$ in weight percent showing a crystallization trend similar to the trend defined by Apollo 12 and Apollo 15 samples (Papike et al., 1998).

Table 3
Major and trace element composition of NEA 003-A and other mare-basalt meteorites and similar Apollo 12 olivine basalts and Apollo 15 olivine-normative basalts.

	Mare-basalt meteorites								Apollo 12 and 15 basalts					
	NEA 003-A CGS	NEA 003-A WUSL	NEA 003-A (−10%)	LAP 02205	Dho 287A	NWA 032	Y-793169	A-881757	12012,15	12040,36	12015,9–11	12,009	15016,195	15555,807
wt%														
SiO_2*	44.72		45.54	45.2	43.2	44.7	46	47.1	44.17	43.89	44.98	45	44.6	45
TiO_2*	1.34		1.49	2.72	2.76	3.08	2.19	2.45	2.64	2.74	2.86	2.9	2.24	2.02
Al_2O_3*	8.02		8.93	10	8.35	8.74	11.1	10	7.71	7.41	8.57	8.59	8.54	9.16
Cr_2O_3*	0.52	0.59	0.58	0.19	0.65	0.4	0.24	0.29	0.69	0.74	0.68	0.76	0.84	0.74
FeO*	21.83	19.3	21.56	23.2	22.1	23	21.2	22.5	20.69	20.83	20.18	21	21.74	21.49
MnO*	0.27		0.3	0.23	0.29	0.33	0.32	0.34	0.3	0.26	0.29	0.28	0.28	0.28
MgO*	13.59		10.97	5.99	13.2	8.45	5.75	6.3	14.37	16.1	11.88	11.6	11.22	11.32
CaO*	9.16		10.19	11.2	8.74	10.9	12	11.8	8.47	7.87	9.21	9.42	9.37	9.47
Na_2O**	0.31	0.262	0.34	0.33	0.53	0.37	0.27	0.25	0.21	0.2	0.23	0.23	0.22	0.23
K_2O**	0.08	<0.3	0.09	0.11	0.19	0.11	0.06	0.04	0.06	0.04	0.06	0.06	0.04	0.05
Total	99.84		99.99	99.83	100.01	100.08	99.13	101.07	99.31	100.08	98.94	99.84	99.09	99.76
Mg#	52.6		47.6	31.4	51.5	39.6	32.6	33.3	55.3	57.9	51.2	49.6	47.9	48.4
μg/g														
Sc		50.8		58.6	35.2	56	93.7	99.4	41.9	42.6	48.4	46	40.7	39.1
Co		50.5		37.3	42.3	42	29.8	27.9	56	59.5	47.8	50.1	54.6	55.4
Ni		84		27.6	20	50	53	52	60	101	62	55	72	67
Sr		117		135.3	530	142	78	115	89	94	84	86.4	90	90
Ba		252		164.7	200	242	34	27	56	54	65	55.5	57	39
La		3.0		13.4	12.9	11.2	4.72	3.69	—	4.3	6.2	5.62	5.22	3.88
Ce		8.5		37.31	30.3	29.7	14.8	10.9	13.8	12.5	16	16.1	15.2	11.6
Nd		4.5		25.12	20.4	21	11.9	8.31	—	8.8	14.4	12.7	8	8
Sm		1.69		7.56	6.31	6.61	4.3	2.88	4.02	3.1	4.3	3.91	3.67	2.78
Eu		0.6		1.24	1.18	1.1	1.31	1.1	0.76	0.79	0.98	0.89	0.82	0.78
Tb		0.46		1.93	1.22	1.56	1.02	0.76	1.17	0.92	1.16	0.9	0.82	0.6
Yb		1.94		6.37	3.35	5.79	4.59	3.26	3.4	2.9	3.6	3.05	2.18	1.77
Lu		0.28		0.88	0.51	0.8	0.66	0.52	0.47	0.37	0.52	0.45	0.31	0.25
Hf		1.1		5.39	2.64	5	3.01	2.2	3.4	2.4	3.3	—	2.49	2.03
Ta		0.15		0.77	0.71	0.62	0.31	0.22	—	0.3	0.38	0.3	0.37	0.29
Th		0.43		2.33	0.9	1.9	0.68	0.42	0.67	0.47	0.74	0.85	0.41	0.29
U		0.29		0.55	—	0.45	0.09	0.16	—	—	—	0.23	—	—

Analytical data of NEA 003-A were acquired by using XRF (∗) and ICP-OES (∗∗) in Czech Geological Survey (CGS) and by INAA in Washington University, St. Louis (WUSL). NEA 003-A (−10%) is recalculated bulk-composition after 10% olivine removal for crystallization modelling.

Other data sources: LAP 02205 (Anand et al., 2006), Dhofar 287A (Anand et al., 2003), NWA 032 (Fagan et al., 2002), Yamato 793169 (Warren and Kallemeyn, 1993; Koeberl et al., 1993), Asuka 881757 (Warren and Kallemeyn, 1993; Koeberl et al., 1993), Apollo 12 olivine basalts: 12012,15, 12015,9–11 (Rhodes et al., 1977), 12040,36 (Neal et al., 1994) and 12009 (Snyder et al., 1997), Apollo 15 olivine normative basalts: 15555,807 and 15016,195 (Ryder and Schuraytz, 2001).

liquid) of Delano (1980). The calculated TiO_2 K_d for NEA 003-A is 0.33 and the Fo content of olivine in NEA 003-A with Mg# = 52.6 (Table 3) is calculated to be Fo_{77}. However, the highest observed Fo content in the cores of the earliest formed olivines (Fo_{73}) is lower than the calculated Fo content. This discrepancy, combined with other geochemical features (high MgO and low Al_2O_3 concentrations, and high Co/Sc ratio), is indicative of the presence of cumulate olivine and its accumulation in the parental magma. Thus, prior to modelling the crystallization sequence, the proportion of cumulate olivine was calculated (equilibrium Fo content = measured Fo content) and corresponds to a value of 10%. This olivine portion was removed, and the bulk composition of NEA 003-A was recalculated (see Table 3). The recalculated bulk-rock composition was used for crystallisation modelling using the PELE software (Boudreau, 1999) based on the algorithms and database of Ghiorso (1985) and Ghiorso and Sack (1994).

The results of low-pressure (1-bar) models of the crystallization sequence for equilibrium and fractional crystallization provide consistent datasets. Modelling started with a liquidus temperature of 1334 °C and an oxygen fugacity equivalent to the iron–wüstite buffer. When comparing both models, fractional crystallization yields better fit between predicted and observed compositional ranges for most mineral phases. This is consistent with other lines of evidence for fractional crystallization of this rock (e.g. type of chemical zonation for olivine, pyroxene and plagioclase—see Sections 3.2.1–3.2.3, strong REE variations be-

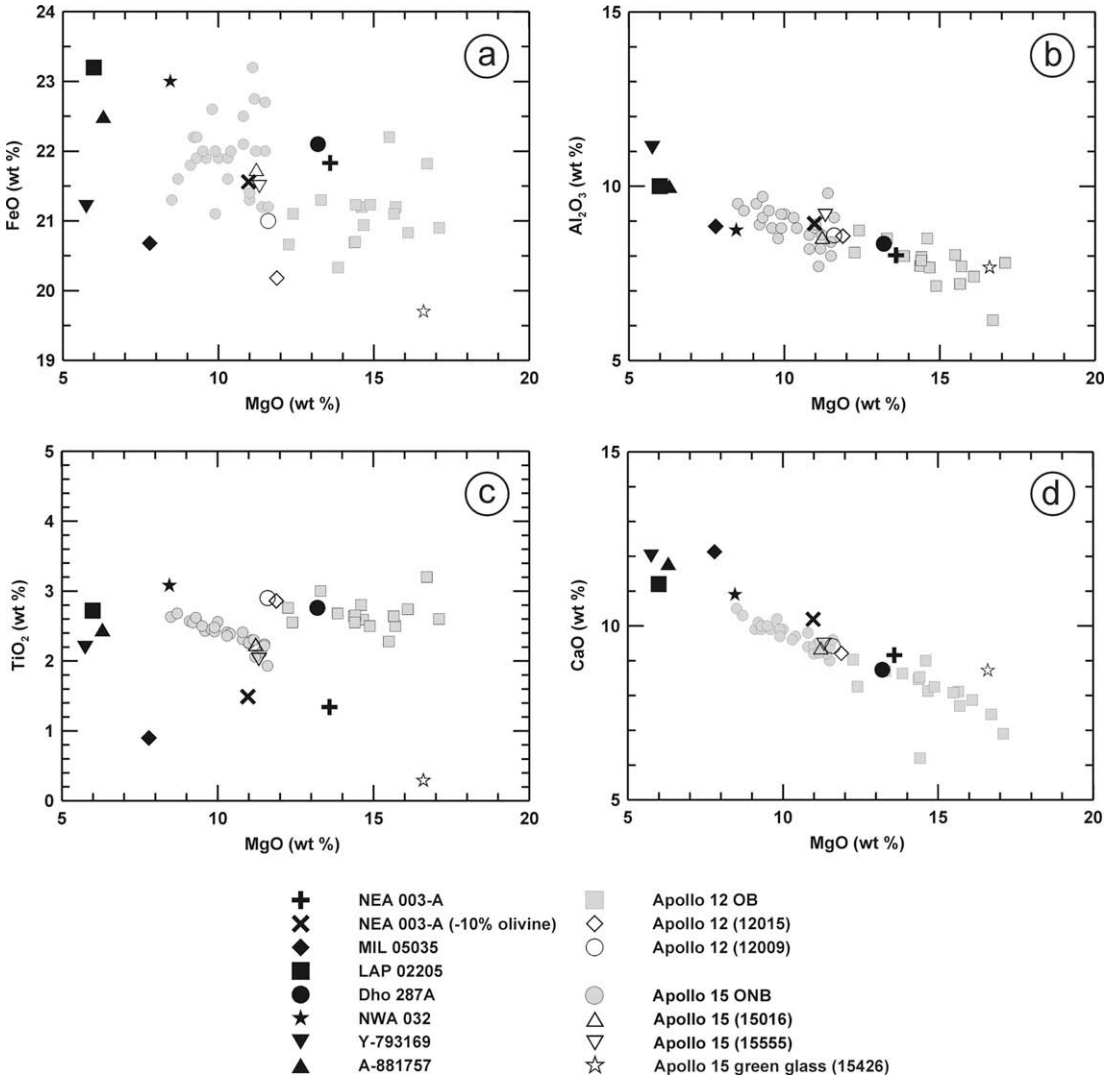

Fig. 8. Major element chemistry of NEA 003-A compared with selected unbrecciated mare-basalt meteorites and Apollo 12 olivine basalts and Apollo 15 olivine-normative basalts. Data sources: NEA 003-A (this study), Miller Range (MIL) 05035 (Joy et al., 2008), LAP 02205 (Anand et al., 2006), Dhofar 287A (Anand et al., 2003), NWA 032 (Fagan et al., 2002), Yamato 793169 (Warren and Kallemeyn, 1993), Asuka 881757 (Warren and Kallemeyn, 1993), Apollo 12 olivine basalts (Rhodes et al., 1977; Neal et al., 1994), Apollo 15 olivine-normative basalts (Ryder and Schuraytz, 2001) and Apollo 15 green glass: 15426 (Taylor et al., 1973).

tween core and rim for pyroxene and plagioclase grains—see Section 3.5.1). The low-pressure model of fractional crystallization for the recalculated bulk composition of NEA 003-A (Fig. 11) predicts that chromian-spinel crystallized as the first phase from the cooling liquid at 1334 °C, followed by olivine (Fo_{73}) at 1241 °C, pigeonite (En_{71}, Wo_6) at 1171 °C, plagioclase (An_{87}) at 1148 °C, clinopyroxene (En_{63}, Wo_{26}) at 1130 °C and ilmenite at 1032 °C. The predicted and observed compositional ranges of mineral phases are in good agreement, with the exception of plagioclase where the compositional range is more scattered (observed An_{84-92}, predicted An_{86-88}). This difference may be a result of compositional zoning in plagioclase however it is not significant for the interpretation of crystallization history. In addition, the difference between the observed and predicted chemical compositions of plagioclase cannot be a result of total conversion to maskelynite during shock process(es) because plagioclase grains show normal magmatic zoning without any homogenization of chemical composition.

The results of crystallization modelling of NEA 003-A described above confirms the presence of cumulate olivine and its accumulation in parental magma and is also consistent with the crystallization sequence derived from Ti and Al variations in pyroxenes (Section 3.2.2 and Fig. 5b).

The chemical zoning preserved in olivine crystals provides information about the cooling-rate during crystallization. The variations of Fo content in 12 olivine grains, measured along mutually orthogonal profiles across the grains, were used to estimate the minimum cooling rates. The effects of crystallographic orientation on Mg–Fe diffusion in the olivine grains was taken into account in the calculation (Taylor et al., 1977). Minimum cooling rate estimates based on the variation of Fo content in olivine crystals require iterative

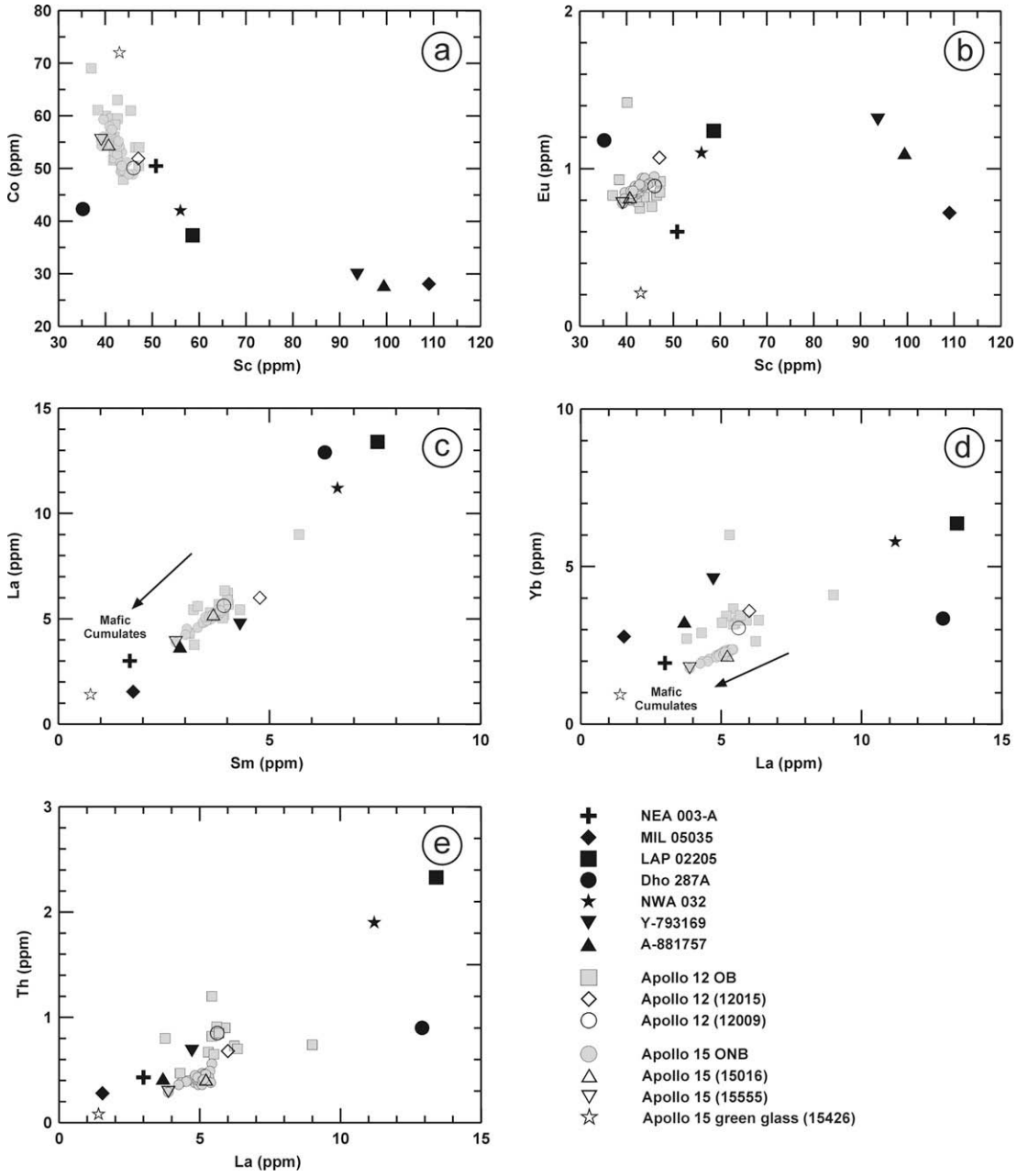

Fig. 9. Trace element chemistry of NEA 003-A compared with selected unbrecciated mare-basalt meteorites and Apollo 12 olivine basalts and Apollo 15 olivine-normative basalts. Data sources: NEA 003-A (this study), Miller Range (MIL) 05035 (Joy et al., 2008), LAP 02205 (Anand et al., 2006), Dhofar 287A (Anand et al., 2003), NWA 032 (Fagan et al., 2002), Yamato 793169 (Koeberl et al., 1993), Asuka 881757 (Koeberl et al., 1993), Apollo 12 olivine basalts (Rhodes et al., 1977; Neal et al., 1994), Apollo 15 olivine-normative basalts (Ryder and Schuraytz, 2001) and Apollo 15 green glass: 15426 (Taylor et al., 1973).

calculations (Taylor et al., 1977). Based on this procedure, the calculated minimal cooling rate for the randomly oriented olivine crystals was ~0.07 °C/h.

3.5. Age determination

3.5.1. Sm–Nd results

We have analyzed five mineral fractions for their Sm–Nd isotope compositions. The analytical results are listed in Table 4a and plotted in an isochron diagram in Fig. 12.

Samarium and Nd concentrations and Sm/Nd ratios are generally well within the range expected from REE distribution coefficients and fractionation models for plagioclase–clinopyroxene pairs (e.g. Jacobsen and Wasserburg, 1979, and references therein), as well as experimentally determined values in Ca-feldspar–pyroxene pairs of terrestrial mafic systems, or ancient lunar samples (Nyquist et al., 1989; Nyquist and Shih, 1992; Premo and Tatsumoto, 1992), with slight variations among the clinopyroxene fractions.

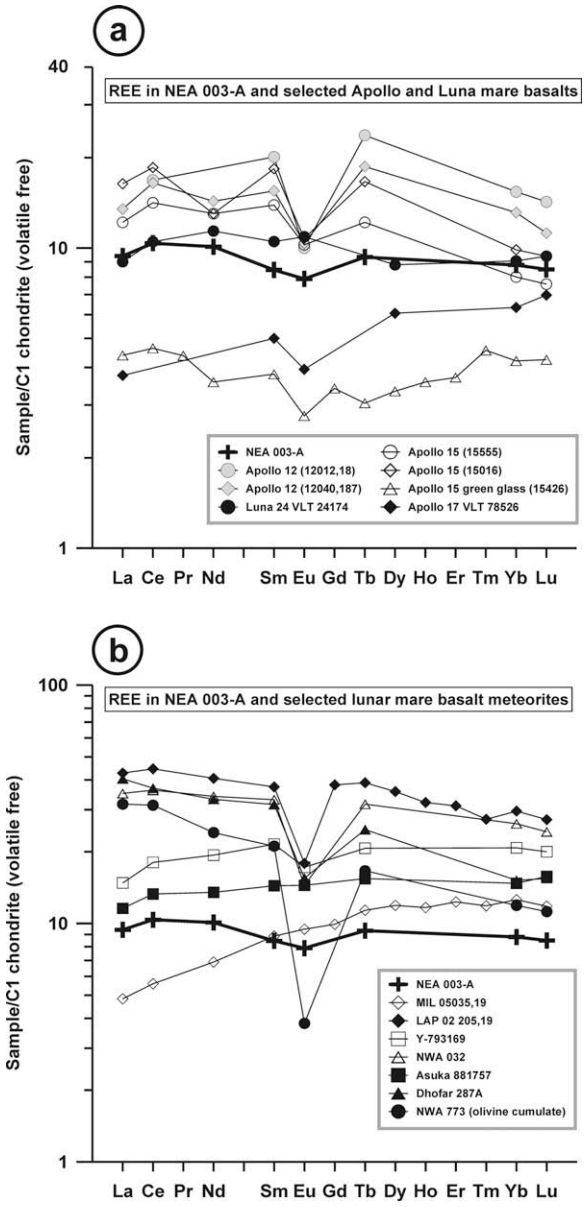

Fig. 10. (a) Volatile-free, chondrite-normalized plot of REEs in NEA 003-A and selected Apollo and Luna mare basalts. (b) Volatile-free, chondrite-normalized plot of REEs in NEA 003-A and selected mare-basalt meteorites. Normalization values are from Anders and Grevesse (1989). *Data sources:* Apollo 12 basalts: 12012,18 (Rhodes et al., 1977) and 12040,187 (Neal et al., 1994), Apollo 15 basalts: 15555 and 15016 (Ryder and Schuraytz, 2001), Apollo 15 green glass: 15426 (Taylor et al., 1973), Apollo 17 (Wentworth et al., 1979), Luna 24 (Ma et al., 1978), Asuka 881757 (Koeberl et al., 1993), Yamato 793169 (Koeberl et al., 1993), LAP 02205 (Anand et al., 2006), Dhofar 287A (Anand et al., 2003), NWA 032 (Fagan et al., 2002), Miller Range 05035 (Joy et al., 2008) and NWA 773 (Jolliff et al., 2003).

The $^{147}Sm/^{144}Nd$ ratios determined in our study for pure plagioclase (Pl) and clinopyroxene (Cpx) are 0.169 and 0.321, respectively (Table 4a). The relatively low Nd and Sm concentrations in the Cpx fraction (Table 4a) are due to a considerable amount of admixed olivine. As expected

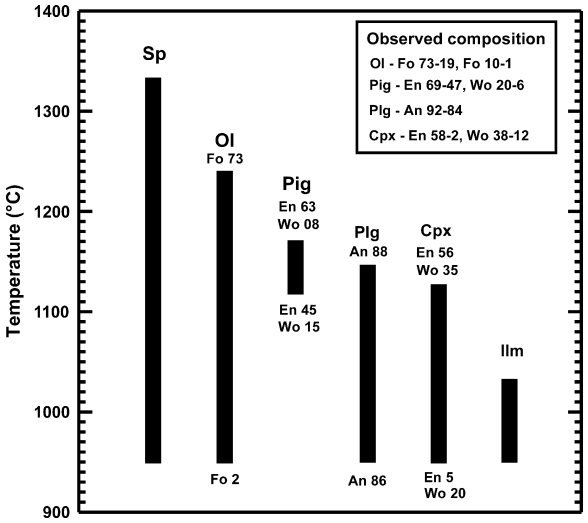

Fig. 11. Results of fractional crystallization modelling of the NEA 003-A recalculated bulk-rock composition (Table 3). The figure also shows predicted and observed compositional ranges of the most abundant phases of NEA 003-A (Sp, spinel; Ol, olivine; Pig, pigeonite; Plg, plagioclase; Cpx, clinopyroxene; Ilm, ilmenite).

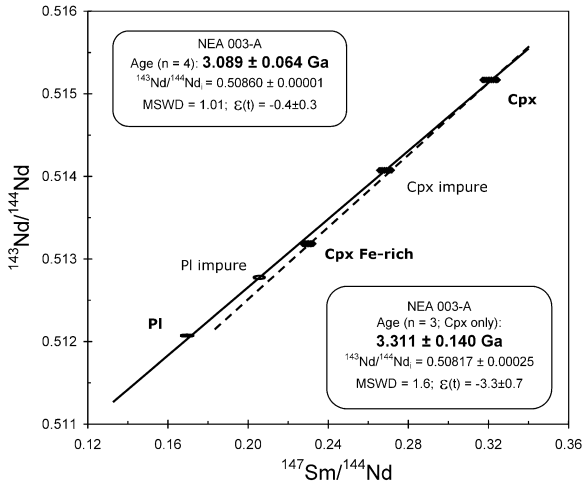

Fig. 12. Sm–Nd isotopic data for mineral fractions of NEA 003-A shown as an isochron diagram. Note that symbol sizes exceed analytical errors. See text for data interpretation. The 3.089 ± 0.064 Ga Sm–Nd regression age (continuous line) is interpreted to be the primary crystallization age of the rock.

from the modal composition, and because plagioclase and clinopyroxene are the major REE-bearing phases, the two impure mineral fractions have an intermediate composition between the pure Pl and Cpx fractions as is evident in the isochron diagram (Fig. 12; and Table 4a). However, the fraction "Cpx impure" may also include a REE-rich accessory phase with a lower Sm/Nd (likely ilmenite or apatite, since its Nd concentration of 5 ppm is considerably higher compared to the "pure" Cpx, Nd = 1.69 ppm; Table 4a). The fraction "Cpx–Fe-rich" has a lower $^{147}Sm/^{144}Nd$ of 0.23 (Table 4a) compared to the "pure" Cpx fraction, which also suggests that clinopyroxene must be strongly zoned with respect to trace elements (REE).

The LA-ICP-MS was used to document the suggested REE zonation of minerals, used for age determination. The REE concentrations were measured for core and rim of selected clinopyroxene and plagioclase grains. The results are presented in Table 5. Clinopyroxene and plagioclase show significant variations: clinopyroxene core and rim have 0.5–5.8 ppm Nd and 0.4–1.7 ppm Sm whereas plagioclase core and rim have 0.3–2.0 ppm Nd and 0.2–0.5 ppm Sm, respectively. The high trace element variations in pyroxene and plagioclase can be attributed to a relatively long period of crystallization for both phases. In addition, trace element enrichment from core to rim of pyroxene and plagioclase indicates fractional crystallization of NEA 003-A from parent melt.

Fig. 12 shows that four out of five data points (Cpx, Cpx impure, Pl impure, Pl) plot on a linear array (solid line). If pooled together in one single regression calculation the age obtained is $t = 3.089 \pm 0.064$ Ga, with $(^{143}Nd/^{144}Nd)_i = 0.508610 \pm 0.000095$ and $\varepsilon_{Nd3089} = -0.4 \pm 0.3$ (MSWD = 1.01). Within the limits of analytical uncertainties, this age corresponds to an isochron. A separate regression of the "pure" Pl and Cpx fractions yields an identical, two-point isochron result of $t = 3.096 \pm 0.073$ Ga, $(^{143}Nd/^{144}Nd)_i = 0.50861 \pm 0.00010$ corresponding to $\varepsilon_{Nd3096} = -0.1 \pm 0.3$. The two low-Sm/Nd fractions (Pl–Pl impure) yield a younger apparent age of 2.94 ± 0.22 Ga. This value is, however, indistinguishable within the uncertainty from the more precise age. Interestingly, Cpx–Fe-rich plots clearly off the 3.1 Ga "mean" trend line. If Cpx–Fe-rich fraction is regressed with the Cpx fraction, it defines an age of 3.30 ± 0.14 Ga and an initial $^{143}Nd/^{144}Nd$ of 0.50817 ± 0.00025, corresponding to a significantly more negative $\varepsilon_{Nd3.3}$ of -3.4 ± 0.7. If the fraction "Cpx impure" is also included (dashed line), the result is identical: $t = 3.31 \pm 0.14$ Ga, $(^{143}Nd/^{144}Nd)_i = 0.50817 \pm 25$ ($\varepsilon_{Nd3.31} = -3.3 \pm 0.7$; MSWD = 1.6). Inclusion of all five data points in one single regression, yields $t = 3.107 \pm 0.240$ Ga ($\varepsilon_{Nd3.1} = -0.9 \pm 1$), with considerable excess scatter (MSWD = 6.3).

For reasons discussed later in Section 4.2, we consider the age of 3.089 ± 0.064 Ga, $(^{143}Nd/^{144}Nd)_i = 0.508610 \pm 0.000095$, $\varepsilon_{Nd3089} = -0.4 \pm 0.3$, and MSWD = 1.01 to best represent the crystallization age of NEA 003-A.

3.5.2. Ar–Ar results

The Ar–Ar data for bulk samples and plagioclase and pyroxene separates are given in Table 4b and the age and Ca/K spectra are shown in Fig. 13a and 13b. The $^{38}Ar/^{36}Ar$ ratios range from ~0.19 at low temperature to 1.6 at high temperature suggesting that Ar is a mixture of trapped and cosmogenic components. At low temperature, the lack of ^{39}Ar release associated with high $^{40}Ar/^{36}Ar$ ratios indicates that that trapped Ar is more likely to be terrestrial atmosphere associated with weathering rather than solar Ar. The absence of solar Ar suggests that NEA 003-A was not directly exposed at the lunar surface throughout its history.

Age spectra for the two bulk samples (Fig. 13a) do not overlap probably because the relatively coarse-grain size of this basalt means that the smaller sample used for laser-heating is unlikely to be representative of the bulk meteorite. However, the similarity in the age pattern between the laser-heated bulk-rock and the pyroxene separates (Fig. 13b) is consistent with pyroxene being the most abundant mineral phase in this sample. The age spectra of the two bulk samples (in particular the laser step heated sample) and the pyroxene separate are similar showing increasing apparent ages over the initial 15–30% of ^{39}Ar release, reaching a maximum value of 2.781 ± 0.058 Ga at 950 °C (the maximum age for the laser step heating of the bulk sample is 3.052 ± 0.588 Ga), followed by a decrease in apparent age over the remaining ^{39}Ar release to <2 Ga. At high temperature, the apparent ages decrease markedly to ~1.2 Ga. The pattern of Ca/K values shows the opposite pattern to the apparent ages, steadily increasing with temperature (Fig. 13a and b). The pyroxene is chemically zoned for Ca and K (Table 2). Thus, most of the variation in Ca/K value may be attributed to the chemical zonation as

Table 4
(a) Sm–Nd analytical results of NEA 003-A mineral separates. (b) Summary of ^{40}Ar–^{39}Ar age data for bulk, breccia and basalt fragments of NEA 003-A.

Material	Sample wt. (mg)	Sm (ppm)	Nd (ppm)	$^{147}Sm/^{144}Nd$	$^{143}Nd/^{144}Nd$	$\pm 2s_m$
(a) Sm–Nd results						
PI	22.6	0.188	0.671	0.1695	0.512073	0.0000087
PI impure	34.2	0.564	1.663	0.2057	0.512777	0.0000170
Cpx	32.06	0.897	1.692	0.3208	0.515168	0.0000040
Cpx impure	36.62	2.238	5.039	0.2686	0.514074	0.0000040
Cpx–Fe-rich	2.3	2.870	7.548	0.2299	0.513185	0.0000060

Material	Sample wt. (mg)	K (ppm)[a]	Ca (%)[a]	Total age (GA)	CRA age (Ma)
(b) Ar–Ar results					
Bulk-IR	2.11	160	4.8	1.744 ± 0.070	212.3 ± 7.5
Bulk-furnace	17.65	327	7.6	2.314 ± 0.040	206.0 ± 6.3
Maskelynite-separates	3.86	112	4.2	2.418 ± 0.044	202.8 ± 3.1
Pyroxene-separates	0.98	90	2.8	1.745 ± 0.060	209.0 ± 4.9

The ^{40}Ar–^{39}Ar age data were obtained by IR-stepped heating. Calculated ages show error in 2σ which includes error for *J*-value determination.

[a] K and Ca content reported were calculated based on the ^{39}Ar and ^{37}Ar released during laser heating.

Table 5
REE concentrations of selected pyroxene and plagioclase grains.

Phases	Pyroxene (En_{61} Wo_{13})		Pyroxene (En_{48} Wo_{35})		Pyroxene (En_{29} Wo_{22})		Pyroxene (En_{8} Wo_{26})		Plagioclase (An_{91})		Plagioclase (An_{89})		Plagioclase (An_{86})	
ppm		±1σ		±1σ		±1σ		±1σ		±1σ		±1σ		±1σ
La	0.11	0.02	0.10	0.02	0.36	0.06	1.86	0.10	0.32	0.02	0.36	0.02	1.31	0.05
Ce	0.33	0.03	0.49	0.04	1.48	0.14	6.08	0.26	0.70	0.03	0.86	0.03	3.15	0.10
Pr	0.04	0.01	0.10	0.02	0.36	0.06	1.01	0.04	0.08	0.01	0.11	0.01	0.43	0.02
Nd	0.54	0.09	0.87	0.12	2.17	0.38	5.78	0.21	0.33	0.03	0.52	0.04	2.01	0.09
Sm	0.38	0.09	0.70	0.13	0.67	0.27	1.65	0.19	0.20	0.08	0.24	0.09	0.54	0.09
Eu	0.03	0.01	0.05	0.02	0.17	0.07	0.45	0.03	1.29	0.05	1.44	0.06	1.44	0.06
Gd	0.50	0.15	1.19	0.22	2.32	0.61	2.70	0.15	0.12	0.03	0.11	0.04	0.73	0.07
Tb	0.16	0.02	0.23	0.03	0.49	0.08	0.53	0.02	0.02	<0.01	0.04	0.01	0.11	0.01
Dy	0.98	0.11	2.09	0.19	3.22	0.36	4.12	0.16	0.07	0.01	0.08	0.02	0.88	0.05
Ho	0.25	0.03	0.55	0.05	0.72	0.10	0.93	0.03	0.02	<0.01	0.01	<0.01	0.16	0.01
Er	0.74	0.09	1.56	0.14	2.23	0.29	2.80	0.10	0.02	<0.01	0.06	0.01	0.48	0.03
Tm	0.11	0.02	0.24	0.03	0.37	0.08	0.44	0.03	0.03	0.01	0.04	0.01	0.06	0.02
Yb	0.81	0.10	1.69	0.18	2.51	0.39	3.17	0.13	0.03	0.01	0.06	0.01	0.38	0.03
Lu	0.13	0.02	0.26	0.03	0.41	0.08	0.50	0.02	0.01	<0.01	0.01	<0.01	0.04	0.01

opposed to release from different mineral phases. In contrast to pyroxene, the apparent age and Ca/K spectra for maskelynite (Fig. 13b) are relatively flat with apparent ages of between 2.0 and 2.5 Ga. The complexities of shock on the Ar system in NEA 003-A are unknown but different minerals may have experienced both Ar loss by diffusion during shock heating and Ar gain by shock implantation. For this reason we consider only total ages obtained by integrating Ar released by all the temperature steps. Total ages are reported in Table 4b and range between 1.8 (pyroxene) to 2.4 Ga (maskelynite, bulk).

Cosmic ray exposure (CRE) age spectra are relatively flat for 84–94% of the $^{37}Ar_{Ca}$ release (Fig. 13c). Using the equations of Eugster and Michel (1995) and taking into account the contribution from Ca, Fe, Ti, Cr, Mn, K and Ni (from Table 3), a ^{38}Ar production rate of 1.013×10^{-8} cc/g/Ma is obtained for a 2π exposure (i.e. exposure on the lunar surface only). This production rate gives CRE plateau ages between 206 and 212 Ma, with a weighted average of 209 ± 6 Ma (Fig. 13c, Table 4b). The lack of trapped solar Ar in NEA 003-A means that the CRE ages should be regarded as the minimum period of residence in the upper regolith of this meteorite.

4. DISCUSSION

4.1. Comparison with other lunar basalts

4.1.1. Apollo and Luna basalts

NEA 003-A, classified as low-Ti, low-Al, low-K olivine mare-basalt, has a major element composition close to low-Ti olivine mare basalts from Apollo 12 and low-Ti olivine-normative basalts from Apollo 15 (Fig. 8). However, the majority of Apollo 12 olivine basalts and Apollo 15 olivine-normative basalts are richer in TiO_2 (Fig. 8c) compared to NEA 003-A. Furthermore, Apollo 12 basalts often contain cumulate olivine (Walker et al.,1976) with higher MgO and lower Al_2O_3 and CaO concentrations (Fig. 8b, d) than those in NEA 003-A.

As demonstrated by crystallisation modelling (Section 3.4), a portion of the olivine in NEA 003-A is of cumulate origin and its highest Fo content is not in equilibrium with whole rock Mg#. For the comparison with other lunar basalts we removed the corresponding portion (~10%, see Section 3.4) of olivine cumulate content from the meteorite bulk-rock composition. The recalculated NEA 003-A bulk composition (Table 3) therefore reflects the character of the parental magma without any influence from the cumulate component. Most Apollo 12 olivine basalts show a similar discrepancy between measured Fo content of olivine cores and calculated equilibrium Fo content, indicating that a portion of the olivine in these rocks is also of cumulate origin (Rhodes et al., 1977; Neal et al., 1994). Ryder and Schuraytz (2001) calculated the amount of olivine separation or addition that dominates the chemical differences among most of the Apollo 15 olivine-normative mare basalts to be 15%. However, they conclude that none of the analyzed rocks in their study show any evidence of significant olivine accumulation.

Comparing the recalculated bulk composition of NEA 003-A (Table 3) with the compositions of similar Apollo 12—12,009 and 12,015 olivine basalts (without cumulate component; Rhodes et al., 1977; Lindstrom and Haskin, 1978) show that there are some similarities but the TiO_2 concentration and Mg# value for 12,009 and 12,015 basalts are higher (Table 3 and Fig. 8c). Moreover, the different trace element compositions (discussed below) reveal that there is not much evidence for a possible connection with the evolution of Apollo 12 olivine basalts. The recalculated bulk composition of NEA 003-A shows a better match to Apollo 15 samples 15,016 and 15,555 olivine-normative basalts, where TiO_2 concentrations and Mg# values are close to NEA 003-A (Table 3 and Fig. 8c). We propose that NEA 003-A bears a close similarity to Apollo 15 olivine-normative basalts with respect to their major element compositions.

The whole-rock trace-element composition of NEA 003-A is characterized by lower REE concentrations (Table 3) and a less pronounced Eu anomaly than Apollo 12 and Apollo 15 basalts (Fig. 10a). NEA 003-A is depleted in light REE (LREE) and plots of La vs. Yb and Sm vs. La (Fig. 9c and d) show that concentrations of LREE approach the

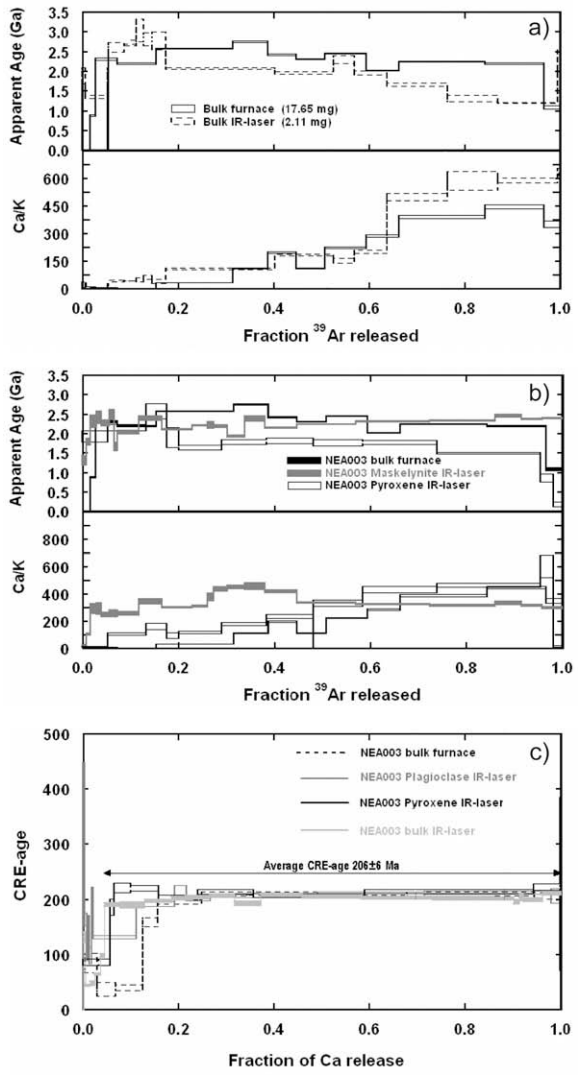

Fig. 13. Apparent age and Ca/K vs. fraction of ^{39}Ar released during step heating for NEA 003-A: (a) bulk samples; and (b) pyroxene and maskelynite separates. (c) Cosmic ray exposure (CRE) age vs fraction of Ca released for bulk, pyroxene and maskelynite samples.

composition of Apollo 15 olivine-normative basalts following the trend of mafic cumulates (Neal and Taylor, 1992). The LREE concentrations of Apollo 12 olivine basalts follow the same trend (Fig. 9c and d), but are obviously higher than for NEA 003-A and Apollo 15 olivine-normative basalts (Neal et al., 1994). The low incompatible trace element concentration of NEA 003-A (Table 3) indicates an absence of a significant KREEP component and also that NEA 003-A is generally more geochemically primitive than Apollo 15 olivine-normative basalts and Apollo 12 olivine basalts, but with a closer relationship with the former. It is therefore possible that NEA 003-A represents an unknown geochemically primitive member of the Apollo 15 olivine-normative basalt series.

We suggest that NEA 003-A parent melt was derived from primitive picritic magma by magmatic differentiation processes. The evidence of a primitive chemical composition of NEA 003-A with low REE concentration, near chondritic initial Nd isotopic ratios very similar to Apollo 15 green glasses (see Section 4.2 for more discussion), with no geochemical evidence for hybridization of the parent melt by magma mixing and assimilation processes supports this hypothesis.

4.1.2. Mare-basalt meteorites

Among unbrecciated low-Ti mare-basalt meteorites, NEA 003-A has a similar modal mineralogy and major element composition to Dhofar 287A. Dhofar 287A also contains a significant portion of cumulate olivine. However, the alkali content and trace element geochemistry (Th and REE concentration) of both meteorites are different due to the presence of a KREEP component in Dhofar 287A (Anand et al., 2003).

NEA 003-A has the highest concentration of Co and the lowest concentration of Eu among the unbrecciated low-Ti mare-basalt meteorites (Fig. 9a and b and Table 3) due to its high modal abundance of olivine and the lowest modal abundance of plagioclase (Table 1). The REE concentrations of NEA 003-A are different from all mare-basalt meteorites with the exception of Kalahari 009. However, Kalahari 009 is a very low-Ti mare-basalt breccia with completely different composition, origin and evolution (Schulz et. al., 2007; Terada et al., 2007; Sokol et al. 2008).

On the basis of its geochemistry, mineralogy and petrology, crystallization age and cosmic ray exposure age, NEA 003-A represents a new type of mare-basalt which is not paired with any other previously described lunar meteorites. We conclude that NEA 003-A represents a previously unknown type of low-Ti mare-basalt that was probably derived from a chemically similar magma source to Apollo 15 olivine-normative basalts.

4.2. Crystallization and shock ages

The apparent four-point Sm–Nd regression age of 3.089 ± 0.064 Ga calculated for different mineral separates, has a good fit (MSWD = 1.01) indicating that the age has chronological significance (Fig. 12). This 3.09 ± 0.06 Ga age is at the lower end of the age range for low-Ti and/or aluminous lunar basalts from Apollo missions (e.g. Shih et al., 1987; Nyquist and Shih, 1992). However, the "Cpx–Fe-rich" fraction is slightly outside analytical uncertainties of this age and could also bear important chronological information. The 3.3 ± 0.14 Ga age (calculated for the clinopyroxene fractions alone; Fig. 12) would suggest that Cpx may have retained its primary, or at least a more pristine, Sm–Nd age. The discrepancy in Sm–Nd age could then be explained by partial disturbance or re-setting of the Sm–Nd system during the shock processes which converted plagioclase into maskelynite. However, a recent study of Gaffney et al. (2007) suggests no or very little effect of shock metamorphism on the Sm–Nd systematics of Apollo basalt samples even at shock pressures of up to 55 GPa. Furthermore, the shock event(s) forming maskelynite was fast with little heating, since there is no petrographic evidence of recrystallization. The supposed post-shock temperature of

200–250 °C (Stöffler and Grieve, 2007) would have been insufficient to cause Sm–Nd diffusion since the closure temperatures for pyroxene and plagioclase are much higher. The olivines, pyroxenes and plagioclases/maskelynites retained their normal (igneous) zoning and thus the chemical equilibration of divalent major cations was not achieved during the shock metamorphism. It is unlikely that, under these conditions, diffusion of trivalent Sm and Nd took place, and thus ions were not re-distributed and the Sm–Nd system remained closed.

Alternatively, the Sm–Nd system could be influenced by terrestrial contamination due to weathering processes taking place in the hot desert environment where the meteorite was found. Detailed study of individual mineral phases under SEM and using EMPA revealed the presence of large numbers of shock fractures within olivine and pyroxene grains. BSE images show that these fractures are filled with secondary weathering products (mainly calcite), particularly in the outer part of olivine and pyroxene grains (Fig. 3). This is in contrast to maskelynite where the fractures are almost absent. It is likely that during preparation of mineral separates these contamination products were not completely eliminated by acid washing. The Fe-rich pyroxene rims represent the most affected region of the pyroxene grains and slight disturbance in Sm–Nd data can be explained by the presence of terrestrial contamination in this separate.

Overall, the low-Ti mare basalts sampled by Apollo and Luna missions on the Moon range in age from 3.08 to 3.37 Ma (Taylor, 1982; Heiken et al., 1991; Shearer et al., 2006). However, some basaltic lunar meteorites (NWA 032/479, LAP 02205 and paired stones, NWA 773 and paired stones) are younger than Apollo and Luna samples (Fagan et al., 2002; Fernandes et al. 2003; Borg et al., 2004; Rankenburg et al., 2007). Their ages together with Sm–Nd age of NEA 003-A (3.09 ± 0.06 Ga) are within the period of lower Eratosthenian lunar volcanic activity (Stöffler and Ryder, 2001).

The low concentration of incompatible elements and low normalized REE content of NEA 003-A would suggest that the chemical composition of the primary melt was not significantly modified by mixing and assimilation processes. The near-chondritic ε_{Nd} value of -0.4 ± 0.3 (or -0.1 ± 0.3, if only the Pl–Cpx pair is considered) suggests that the basaltic melt of NEA 003-A originated from a slightly enriched source (Fig. 14), less fractionated than most depleted Apollo mare basalts. Lunar rocks with ε_{Nd} values similar to NEA 003-A include mare-basalt meteorite Dhofar 287-A (Shih et al., 2002) and Apollo feldspathic basalt 12038 (Nyquist et al., 1981), (Fig. 14). Unlike NEA 003-A, the composition of these latter basalts (high concentrations of incompatible elements, REEs and high alkali content), (Compston et al., 1971; Nyquist et al., 1981; Anand et al., 2003) indicates that the primary rock melts underwent KREEP assimilation processes. Initial Nd isotopic compositions (ε_{Nd} values) of lunar meteorites younger than NEA 003-A (NWA 032/479, LAP 02205 and paired stones, NWA 773 and paired rocks) are distinct from NEA 003-A (Fig. 14).

The chondritic initial Nd isotopic composition together with other geochemical features of NEA 003-A preclude a common origin with Apollo 12 olivine basalts, as was also concluded previously for the low-Ti mare-basalt meteorite LaPaz Icefield 02205 (Rankenburg et al., 2007). However, there is a strong geochemical affinity of NEA 003-A to Apollo 15 olivine-normative basalts and we can assume that a slightly more evolved source magma of Apollo 15 olivine-normative basalts could be derived by fractional crystallisation from a magma source having a similar composition to NEA 003-A. In contrast, the geochemically similar olivine-normative basalts 15555 and 15016 from Apollo 15 suite were derived from isotopically more depleted source than the near-chondritic NEA 003-A (Fig. 14). Most likely the magma source of these rocks evolved separately in isolated geochemically similar reservoirs. These isotopically distinct magma sources with various initial Nd isoto-

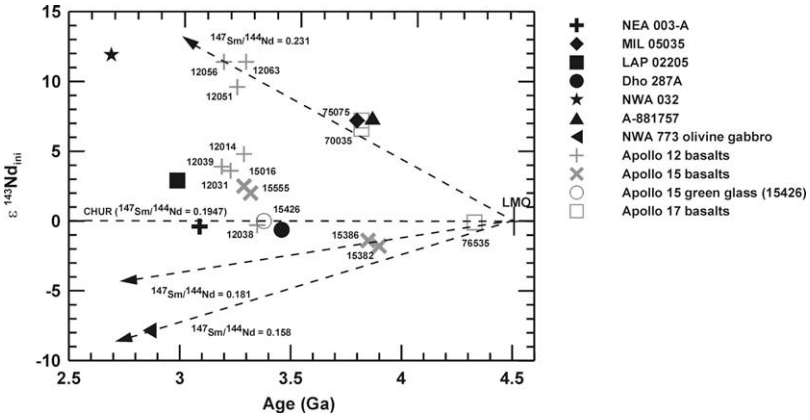

Fig. 14. Initial Nd isotopic composition ε_{Nd} vs age plot for NEA 003-A, mare-basalt meteorites and selected Apollo 12, Apollo 15, and Apollo 17 basalts. The plot indicates that the basaltic melt of NEA 003-A was derived from a very slightly enriched source having $^{147}Sm/^{144}Nd$ ratio very close to CHUR $^{147}Sm/^{144}Nd$ ratio, whereas most of Apollo 12, Apollo 15, and Apollo 17 basalts were derived from a strongly depleted basaltic melt (higher $^{147}Sm/^{144}Nd$ ratio). *Data sources:* NEA 003-A (this study), MIL 05035 (Nyquist et al., 2007), LAP 02205 (Rankenburg et al., 2007), Dhofar 287A (Shih et al., 2002), NWA 032 (Borg et al., 2007), A-881757 (Misawa et al., 1992), NWA 733 olivine gabbro (Borg et al., 2004), Apollo 12, 15 and 17 basalts (Nyquist et al., 1979; Nyquist and Shih, 1992; Nyquist et al., 1995), Apollo 15 green glass: 15426 (Lugmair and Marti, 1978).

pic compositions within Apollo 15 suite were discussed by Nyquist and Shih (1992). The crystallization ages of NEA 003-A (3.09 ± 0.06 Ga) and olivine-normative Apollo 15 basalts ($\sim 3.3 \pm 0.02$ Ga) (Stöffler et al., 2006) are different, but an origin of NEA 003-A during a younger magmatic phase of low-Ti mare-basalt volcanism within the Apollo 15 olivine-normative basalt suite could be envisaged. The near-chondritic ε_{Nd} value of -0.4 ± 0.3 indicates that NEA 003-A could also be derived from a mantle source similar to the Apollo 15 green glass which is also characterized by very low and unfractionated REE abundances (Fig. 10) and near-chondritic Sm/Nd evolution (Lugmair and Marti, 1978). Apollo 15 green glasses are also older (3.38 Ga; Spangler et al., 1984) than NEA 003-A however the basaltic equivalent to these picritic glasses is unknown.

The discordant Ar–Ar and Sm–Nd ages suggest that the K–Ar system was re-set by an impact event at ~1.8 Ga ago. Impact shock was followed by a period of heating sufficient to permit loss of radiogenic ^{40}Ar, but not hot enough to melt plagioclase (<900 °C, e.g. hot ejecta blanket). The Ar–Ar ages from the maskelynite and pyroxene separates are in reverse of what would be expected based upon closure temperature. A tentative explanation for this discrepancy involves an impact event that caused all the minerals to be degassed of their radiogenic ^{40}Ar and re-setting the K–Ar system. During impact the shock features observed in olivine, pyroxene, spinels and the conversion of plagioclase to diaplectic plagioclase glass (maskelynite) developed. This event took place 1.745 ± 0.060 Ga the age obtained from the pyroxene separates), and the shock intensity was of ~28–45 GPa (Stöffler and Grieve, 2007). During the shock event some of the ^{40}Ar released from pyroxene and plagioclase was re-implanted or diffused into maskelynite. This "excess" ^{40}Ar results in relatively old ages (2.418 ± 0.044 Ga) observed for the maskelynite separates as well as those seen for the bulk sample step heated in the Ta-furnace. The process of Ar implantation has been well investigated e.g. Davis (1977), Jessberger and Ostertag (1982), Bogard et al. (1986 and 1989), Wiens and Pepin (1988) and Stephan and Jessberger (1992). These authors suggest that Ar can be implanted at shock pressures as low as 10 GPa due to gas diffusion from pores/cracks into silicates.

It is interesting to note two further observations relevant to the low Ar–Ar ages. Firstly, NEA 003-A and Kalahari 009 are the only two mare-basalt meteorites currently known, in which the K–Ar system has been reset during impact (Sokol et al., 2008); and second that the presence of maskelynite is not incontrovertible evidence that the K–Ar age has been reset. For example, Asuka 881757 shows the presence of maskelynite, however, the Ar–Ar age is within error of the crystallization age obtained by other isotope dating methods (e.g. Sm/Nd, Rb/Sr, U–Th/Pb; Misawa et al., 1992).

5. CONCLUSIONS

1. Crystallization age, cosmic ray exposure age and geochemical and petrological features of NEA 003-A indicate that this meteorite is not paired with any other previously described lunar meteorite. NEA 003-A is a unique low-Ti mare-basalt that is different from Apollo and Luna samples and low-Ti mare-basalt meteorites.

2. The mineralogy, bulk-rock major and trace element composition of NEA 003-A shows similarities with the Apollo 15 olivine-normative basalts. The depletion of REE is indicative of the mafic-cumulate evolution of this rock. It is possible that NEA 003-A represents a previously unknown geochemically primitive type of the Apollo 15 olivine-normative basalt series.

3. Geochemical characteristics (e.g. high Mg#, low concentration of K_2O and Al_2O_3, low concentration of incompatible elements) together with results of crystallization modelling demonstrate the presence of a significant portion of cumulate olivine and suggest that NEA 003-A parent melt was not contaminated by KREEP components during magma mixing and assimilation processes. Low concentrations of incompatible elements also reveal the primitive nature of the parent melt. This parent melt was itself probably derived from a primitive picritic magma by magmatic differentiation processes.

4. Crystallization modelling, the crystallization sequence derived from Ti and Al variations in pyroxenes, and the presence of strong REE variations between core and rim of pyroxene and plagioclase grains, all confirm formation of this rock by fractional crystallization processes. Low minimum cooling rate estimates (~0.07 °C/h) based on the variation of Fo content in olivine suggests that NEA 003-A crystallized in the deeper part of a lava flow in the presence of cumulate olivine.

5. The Sm–Nd crystallization age (3.089 ± 0.064 Ga) corresponds to the period of lower Eratosthenian lunar volcanic activity. Older crystallization ages of geochemically similar Apollo 15 olivine-normative basalts ($\sim 3.3 \pm 0.02$ Ga) indicate that it is possible that NEA 003-A represents a product of younger low-Ti mare-basalt volcanism within the Apollo 15 olivine-normative basalt suite.

6. The initial Nd isotopic composition and near-chondritic ε_{Nd} value (-0.4 ± 0.3) indicate that NEA 003-A could have been derived from a primitive, slightly enriched mantle source that was less fractionated compared to most depleted Apollo mare basalts. The primitive character of NEA 003-A mantle source indicates is similar to that of the Apollo 15 green glass.

7. The discordant Ar–Ar and Sm–Nd ages suggest that the K–Ar system was reset by an impact event at ~1.8 Ga ago with the shock pressures of ~28–45 GPa, that also caused complete conversion of plagioclase to maskelynite. The absence of solar Ar suggests that this impact event did not expose NEA 003-A at the lunar surface and that it remained shielded from galactic cosmic rays and solar wind particles during its lunar history. However, the cosmic ray exposure age of 209 ± 6 Ma implies that NEA 003-A resided in the upper regolith for at least a part of its history.

ACKNOWLEDGMENTS

Franz Brandstätter (Naturhistorisches Museum, Vienna, Austria) and Anton Kearsley (Natural History Museum, London, UK) are thanked for help with EMPA analyses. V.A.F. was funded

by the Fundação para a Ciência e a Tecnologia, Portugal. V.A.F. and R.B. were additionally funded by Particle Physics and Astronomy Research Council and the Royal Society, UK. Tomas Magna (Czech Geological Survey, Prague, Czech Republic) is thanked for critical review of the manuscript. We thank Mahesh Anand (The Open University, Milton Keynes, UK), an anonymous reviewer and Associate Editor Christian Koeberl (University of Vienna, Austria) for constructive comments and suggestions which significantly improved the quality of the paper.

REFERENCES

Anand M., Taylor L. A., Misra K. C., Demidova S. I. and Nazarov M. A. (2003) KREEPy lunar meteorite Dhofar 287A: a new lunar basalt. *Meteorit. Planet. Sci.* **38**, 485–499.

Anand M., Taylor L. A., Floss CH., Neal C. R., Terada K. and Tanikawa S. (2006) Petrology and geochemistry of LaPaz Icefield 02205: a new unique low-Ti mare-basalt meteorite. *Geochim. Cosmochim. Acta* **70**, 246–264.

Anders E. and Grevesse N. (1989) Abundances of the elements: meteoritic and solar. *Geochim. Cosmochim. Acta* **53**, 197–214.

Basaltic Volcanism Study Project (1981) In *Basaltic Volcanism on the Terrestrial Planets*. Chapter 1.2.9: Lunar Mare Basalts. Pergamon Press, Inc., New York, pp. 236–266.

Bogard D., Hörz F. and Johnson P. (1986) Shock-implanted noble gases II: an experimental study with implications for the origin of Martian gases in shergottite meteorites. *J. Geophys. Res.* **91**, E99–E114.

Bogard D., Hörz F. and Johnson P. (1989) Shock-implanted noble gases II: additional experimental studies and recognition in naturally shocked terrestrial materials. *Meteorit. Planet. Sci.* **24**, 113–123.

Borg L. E., Shearer C. K., Asmerom Y. and Papike J. J. (2004) Prolonged KREEP magmatism on the Moon indicated by the youngest dated lunar igneous rock. *Science* **432**, 209–211.

Borg L., Gaffney A. and De Paolo D. (2007) Rb–Sr and Sm–Nd isotopic systematics of NWA 032. *70th Annual Meeting of the Meteoritical Society*, Lunar and Planetary Institute, Houston. #5232 (abstr.).

Boudreau A. E. (1999) A version of the MELTS software program for the PC platform. *Comput. Geosci.* **25**, 21–203.

Clayton R. N. and Mayeda T. K. (1963) The use of bromine pentafluoride in the extraction of oxygen from oxides and silicates for isotopic analysis. *Geochim. Cosmochim. Acta* **27**, 43–52.

Clayton R. N. and Mayeda T. K. (1983) Oxygen isotopes in eucrites, shergottites, nakhlites and chassignites. *Earth Planet. Sci. Lett.* **62**, 1–6.

Compston W., Berry H., Vernon M. J., Chappell B. W. and Kay M. J. (1971) Rubidium-strontium chronology and chemistry of lunar material from the Ocean of Storms. In *Proc. 2nd Lunar Sci. Conf.*, Lunar Planet. Inst., Houston, pp. 1471–1485.

Davis P. K. (1977) Effects of shock pressure on ^{40}Ar–^{39}Ar radiometric age determinations. *Geochim. Cosmochim. Acta* **41**, 195–205.

Day J. M. D., Taylor L. A., Floss C., Patchen A. D., Schnare D. W. and Pearson D. G. (2006) Comparative petrology, geochemistry and petrogenesis of evolved, low-Ti lunar mare basalt meteorites from the LaPaz Icefield, Antarctica. *Geochim. Cosmochim. Acta* **70**, 1581–1600.

Delano J. W. (1980) Chemistry and liquid phase Apollo 15 red glass. Implications for the deep lunar interior. In *Proc. 11th Lunar Sci. Conf.*, Lunar Planet. Inst., Houston, pp. 251–288.

El Goresy A., Ramdohr P. and Taylor L. A. (1971) The opaque minerals in the lunar rocks from Oceanus Procellarum. In *Proc. 2nd Lunar Sci. Conf.*, Lunar Planet. Inst., Houstan, pp. 219–235.

El Goresy A. (1976) Oxide minerals in lunar rocks. In *Oxide minerals* (ed. D. Rumble). Mineralogical Society of America, Washington, DC, pp. EG1–EG43.

Eugster O. and Michel Th. (1995) Common asteroid break-up events of eucrites, diogenites, and howardites and cosmic-ray production rates for noble gases in chondrites. *Geochim. Cosmochim. Acta* **59**, 177–199.

Fagan T. J., Taylor G. J., Keil K., Bunch T. E., Wittke J. H., Korotev R. L., Jolliff B. L., Gillis J. J., Haskin L. A., Jarosewich E., Clayton R. N., Mayeda T., Fernandes V. A., Burgess R., Turner G., Eugster O. and Lorenzetti S. (2002) Northwest Africa 032: product of lunar volcanism. *Meteorit. Planet. Sci.* **37**, 371–394.

Fernandes V. A., Burgess R. and Turner G. (2000) Laser ^{40}Ar–^{39}Ar studies of Dar al Gani 262 lunar meteorite. *Meteorit. Planet. Sci.* **35**, 1355–1364.

Fernandes V. A., Burgess R. and Turner G. (2003) ^{40}Ar–^{39}Ar chronology of lunar meteorites Northwest Africa 032 and 773. *Meteorit. Planet. Sci.* **38**, 555–564.

Fernandes V. A. and Burgess R. (2005) Volcanism in Mare Fecunditatis and Mare Crisium: Ar–Ar studies. *Geochim. Cosmochim. Acta* **69**, 4919–4934.

Gaffney A. M., Borg L. E. and Asmerom Y. (2007) Disturbance of Sm–Nd, Rb–Sr and U–Pb isochrons during shock and thermal metamorphism—an experimental approach. *Lunar Planet. Sci. XXXVIII*. Lunar Planet. Inst., Houston. #1424 (abstr.).

Ghiorso M. S. (1985) Chemical mass transfer in magmatic processes. I. Thermodynamic relations and numerical algorithms. *Contrib. Miner. Petrol.* **90**, 107–120.

Ghiorso M. S. and Sack R. O. (1994) Chemical mass transfer in magmatic processes. IV. A revised and internally consistent thermodynamic model for the interpolation and extrapolation of liquid–solid equilibria in magmatic systems at elevated temperatures and pressures. *Contrib. Miner. Petrol.* **119**, 197–212.

Haloda J., Korotev R. L., Tycova P., Jakes P. and Gabzdyl P. (2006) Lunar meteorite Northeast Africa 003-A: a new lunar mare basalt. *Lunar Planet. Sci. XXXVII*. Lunar Planet. Inst., Houston. #2269 (abstr.).

Hamilton P. J., O'nions R. K., Bridgewater D. and Nutman A. (1983) Sm–Nd studies of Archean metasediments and metavolcanics from West Greenland and their implications for the Earth's early history. *Earth Planet. Sci. Lett.* **62**, 263–272.

Heiken G., Vaniman D. and French B. M., 1991. Lunar Sourcebook. A User's Guide to the Moon. Cambridge University Press, Berlin.

Jacobsen S. B. and Wasserburg G. J. (1979) Nd and Sr isotopic study of the Bay of Islands Ophiolite complex and the evolution of the source of Midocean Ridge Basalts. *J. Geophys. Res.* **84** (B3), 7429–7445.

Jessberger E. K. and Ostertag R. (1982) Shock-effects on the K–Ar system of plagioclase feldspar and the age of anorthosite inclusions from North-Eastern Minnesota. *Geochim. Cosmochim. Acta* **46**, 1465–1471.

Jolliff B. L., Korotev R. L., Zeigler R. A., Floss C. and Haskin L. A. (2003) Northwest Africa 773: lunar mare breccia with a shallow-formed olivine-cumulate component, very-low-Ti (VLT) heritage, and a KREEP connection. *Geochim. Cosmochim. Acta* **67**, 4857–4879.

Jolliff B. L., Hughes J. M., Freeman J. J. and Zeigler R. A. (2006) Crystal chemistry of lunar merrillite and comparison to other meteoritic and planetary suites of whitlockite and merrillite. *Am. Mineral.* **91**, 1583–1595.

Joy K. H., Crawford I. A., Anand M., Greenwood R. C., Franchi I. A. and Russell S. S. (2008) The petrology and geochemistry of Miller Range 05035: a new lunar gabbroic meteorite. *Geochim. Cosmochim. Acta* **72**, 387–402.

Koeberl C., Kurat G. and Brandstätter F. (1993) Gabbroic lunar mare meteorites Asuka-881757 (Asuka-31) and Yamato-793169: geochemical and mineralogical study. In. *Proc. NIPR Symp. Antarct. Meteorites*, vol. **6.** Nat. Inst. Polar Res., Tokyo, pp. 14–34.

Korotev R. L. (2005) Lunar geochemistry as told by lunar meteorites. *Chemie der Erde* **65**, 297–346.

Langmuir C. H. and Hanson G. N. (1981) Calculating mineral–melt equilibria with stoichiometry, mass balance, and single-component distribution coefficients. In *Thermodynamics of Minerals, Melts, Advances in Physical Geochemistry* (eds. R. C. Newton, A. Navrotsky and B. J. Wood). Springer-Verlag, New York, pp. 247–271, vol. 1.

Lindstrom M. M. and Haskin L. A. (1978) Causes of compositional variations within mare basalt suites. In *Proc. 9th Lunar Sci. Conf.*, Lunar Planet. Inst., Houstan, pp. 465–486.

Ludwig K. R. (2003) User's manual for Isoplot 3.00. In *Berkley Geochronology Center Special Publication*, 74 pp.

Lugmair G. W. and Marti K. (1978) Lunar initial $^{143}Nd/^{144}Nd$: differential evolution of the lunar crust and mantle. *Earth Planet. Sci. Lett.* **39**, 3349–3357.

Ma M. S., Schmitt R. A., Taylor G. J., Warner D., Lange D. E. and Keil K. (1978) Chemistry and petrology of Luna 24 lithic fragments and <250 μm soils: constraints on the origin of the VLT mare basalt. In *Mare Crisium: The view from Luna 24* (eds. R. B. Merill and J. J. Papike). Pergamon Press, New York, pp. 569–592.

Misawa K., Tatsumoto M., Dalrymple G. B. and Yanai K. (1992) An extremely low U/Pb source in the Moon: U–Th-Pb, Sm–Nd, Rb–Sr and $^{40}Ar/^{39}Ar$ isotopic systematics and age of lunar meteorite Asuka 881757. *Geochim. Cosmochim. Acta* **57**, 4687–4702.

Neal C. R. and Taylor L. A. (1992) Petrogenesis of mare-basalts: a record of lunar volcanism. *Geochim. Cosmochim. Acta* **56**, 2177–2211.

Neal C. R., Hacker M. D., Snyder G. A., Taylor L. A., Liu Y. G. and Schmitt R. A. (1994) Basalt generation at the Apollo 12 site. Part 1: new data, classification, and re-evaluation. *Meteorit. Planet. Sci.* **29**, 334–348.

Nyquist L. E., Shih C. Y., Wooden J. L., Bansal B. and Wiesmann H. (1979) The Sr and Nd isotopic record of Apollo 12 basalts: Implication for lunar geochemical evolution. *Proc. 10th Lunar Sci. Conf.*, 77–114.

Nyquist L. E., Wooden J. L., Shih C. Y., Wiesmann H. and Bansal B. (1981) Isotopic and REE studies of lunar basalt 12038: Implications for the petrogenesis of aluminous mare basalts. *Earth Planet. Sci. Lett.* **55**, 335–355.

Nyquist L. E., Lindstrom M., Bansal B., Mittlefeldt D., Shih C. Y. and Wiesmann H. (1989) Chemical and isotopic constraints on the petrogenesis of the Large Mare Basalt Clast in Breccia 15459. In *Proc. 19th Lunar Sci. Conf.*, Lunar Planet. Inst., Houstan, pp. 163–174.

Nyquist L. E. and Shih C. Y. (1992) The isotopic record of lunar volcanism. *Geochim. Cosmochim. Acta* **56**, 2213–2234.

Nyquist L. E., Wiesmann H., Bansal B., Shih C. Y., Keith J. E. and Harper C. L. (1995) ^{146}Sm–^{142}Nd formation interval for the lunar mantle. *Geochim. Cosmochim. Acta* **59**, 2817–2837.

Nyquist L. E., Shih C. Y. and Reese Y. D. (2007) Sm–Nd and Rb–Sr ages for MIL 05035: implications for surface and mantle sources. *Lunar Planet. Sci. XXXVIII*. Lunar Planet. Inst., Houston. #2103 (abstr.).

O'nions R. K., Hamilton P. J. and Evensen M. N. (1977) Variations in $^{143}Nd/^{144}Nd$ and $^{87}Sr/^{86}Sr$ in oceanic basalts. *Earth Planet. Sci. Lett.* **34**, 13–22.

Papike J. J., Ryder G. and Shearer C. K. (1998) Lunar samples. In *Planetary Materials* (ed. J. J. Papike). Mineralogical Society of America, Washington, DC, pp. 5-1–5-234.

Papike J. J., Karner J. M. and Shearer C. K. (2003) Determination of planetary basalt parentage: A simple technique using the electron microprobe. *Am. Mineral.* **88**(2–3), 469–472.

Premo W. R. and Tatsumoto M. (1992) U–Th–Pb, Rb–Sr, and Sm–Nd isotopic systematics of lunar Troctolitic Cumulate 76535: implications on the age and origin of this early lunar, deep-seated cumulate. In *Proc. 22th Lunar Sci. Conf.*, Lunar Planet. Inst., Houstan, pp. 381–397.

Rankenburg K., Brandon A. D. and Norman M. D. (2007) A Rb–Sr and Sm–Nd isotope geochronology and trace element study of lunar meteorite LaPaz Icefield 02205. *Geochim. Cosmochim. Acta* **71**, 2120–2135.

Rhodes J. M. and Hubbard N. J. (1973) Chemistry, classification, and petrogenesis of Apollo 15 mare-basalts. In *Proc. 4th Lunar Sci. Conf.*, Lunar Planet. Inst., Houstan, pp. 1127–1148.

Rhodes J. M., Blanchard D. P., Dungan M. A., Brannon J. C. and Rodgers K. V. (1977) Chemistry of Apollo 12 mare basalts: magma types and fractionation processes. In *Proc. 8th Lunar Sci. Conf.*, Lunar Planet. Inst., Houstan, pp. 1305–1338.

Roeder P. L. and Emslie R. F. (1970) Olivine–liquid equilibrium. *Contrib. Miner. Petrol.* **29**, 275–289.

Ryder G. and Schuraytz B. C. (2001) Chemical variation of the large Apollo 15 olivine-normative basalt rock samples. *J. Geophys. Res.* **106**, 1435–1451.

Schmidt N. H. and Olensen N. O. (1989) Computer-aided determination of crystal-lattice orientation from electron-channelling patterns in the SEM. *Can. Mineral.* **28**, 15–22.

Schulz T., Sokol A., Palme H., Weckwerth G., Münker C. and Bischoff A. (2007) Chemical composition and Lu-Hf age of the lunar mare basalt meteorite Kalahari 009. *70th Annu. Meeting Meteor. Soc.,* Lunar and Planetary Institute, Houston. #5151 (abstr.).

Shafer J., Neal C. R. and Castillo P. (2004) Compositional variability in lavas from the Ontong Java Plateau: results from basalt clasts within the volcaniclastic sequence of Ocean Drilling Program Leg 192 Site 1184. In *Origin and Evolution of the Ontong Java Plateau* (eds.J. G. Fitton, J. J. Mahoney, P. J. Wallace and A. D. Saunders), vol. 229. J. Geol. Soc. London Spec. Pub. pp. 333–351.

Shearer C. K., Hess P. C., Wieczorek M. A., Pritchard M. E., Parmentier E. M., Borg L. E., Longhi J., Elkins-Tanton L. T., Neal C. R., Antonenko I., Canup R. M., Halliday A. N., Grove T. L., Hager B. H., Lee D. C. and Wiechert U. (2006) Thermal and magmatic evolution of the moon. In *New views of the Moon* (eds. B. L. Jolliff, M. A. Wieczorek, C. K. Shearer and C. R. Neal). Mineralogical Society of America and Geochemical Society, Washington, DC, pp. 365–518.

Shih C. Y., Nyquist L. E., Bogard D. D., Dasch E. J., Bansal B. M. and Wiesmann H. (1987) Geochronology of high-K aluminous mare basalt clasts from Apollo 14 breccia 14304. *Geochim. Cosmochim. Acta* **51**, 3255–3271.

Shih C. Y., Nyquist L. E., Reese Y., Wiesmann H., Nazarov M. A. and Taylor L. A. (2002) The chronology and petrogenesis of the mare basalt clast from lunarmeteorite Dhofar 287: Rb–Sr and Sm–Nd isotopic studies. *Lunar Planet. Sci. XXXII*. Lunar Planet. Inst., Houston. #1344 (abstr.).

Snyder G. A., Neal C. R., Taylor L. A. and Halliday A. N. (1997) Anataxis of lunar cumulate mantle in time and space. Clues from trace-element, strontium and neodymium isotopic chem-

istry of parental Apollo 12 basalts. *Geochim. Cosmochim. Acta* **61**, 2731–2747.

Sokol A. K., Fernandes V. A., Schulz T., Bischoff A., Burgess R., Clayton R. N., Münker C., Nishiizumi K., Palme H., Schultz L., Weckwerth G. and Mezger K. (2008) Geochemistry, petrology and ages of the lunar meteorites Kalahari 008 and 009: new constraints on early lunar evolution. *Geochim. Cosmochim. Acta* **72**, 4845–4873.

Spangler R. R., Warasila R. and Delano J. W. (1984) ^{39}Ar–^{40}Ar ages for the Apollo 15 green and yellow volcanic glasses. *Proc. 14th Lunar Sci. Conf. J. Geophys. Res* **89**, B487–B497.

Spicuzza M. J., Day J. M. D., Taylor L. A. and Valley J. W. (2007) Oxygen isotope constraints on the origin and differentiation of the Moon. *Earth Planet. Sci. Lett.* **253**, 254–265.

Steiger R. H. and Jäger E. (1977) Subcommission on geochronology: convention on the use of decay constants in geochronology and cosmochronology. *Earth Planet. Sci. Lett.* **36**, 359–362.

Stephan T. and Jessberger E. K. (1992) Isotope systematics and shock-wave metamorphism: III. K–Ar in experimentally and naturally shocked rocks; the Haughton impact structure, Canada. *Geochim. Cosmochim. Acta* **56**, 1591–1605.

Stöffler D. and Ryder G. (2001) Stratigraphy and isotope ages of lunar geologic units: chronological standard for the inner solar system. *Space Sci. Rev.* **96**, 9–54.

Stöffler D., Ryder G., Ivanov B. A., Artemieva N. A., Cintala M. J. and Grieve R. A. F. (2006) Cratering History and lunar Chronology. In *New views of the Moon* (eds. B. L. Jolliff, M. A. Wieczorek, C. K. Shearer and C. R. Neal). Mineralogical Society of America and Geochemical Society, Washington, DC, pp. 519–596.

Stöffler D. and Grieve R. A. F. (2007) Impactites. In *Metamorphic Rocks—A Classification, Glossary of Terms* (eds. D. Fettes and J. Desmons). Cambridge University Press, Cambridge, UK, pp. 82–92.

Takeda H., Arai T. and Saiki K. (1993) Mineralogical studies of lunar meteorite Yamato-793169. In. *Proc. NIPR Symp. Antarct. Meteorites*, vol. **6.** Nat. Inst. Polar Res., Tokyo, pp. 3–13.

Taylor L. A., Kullerud G. and Bryan W. B. (1971) Opaque mineralogy and textural features of Apollo 12 samples and a comparison with Apollo 11 rocks. In *Proc. 2nd Lunar Sci. Conf.*, Lunar Planet. Inst., Houstan, pp. 855–871.

Taylor L. A., Onorato P. I. K. and Uhlmann D. R. (1977) Cooling rate estimations based on kinetic modeling of Fe–Mg diffusion in olivine. In *Proc. 8th Lunar Sci. Conf.*, Lunar Planet. Inst., Houstan, pp. 1581–1592.

Taylor S. R., Gorton M. P., Muir P., Nance W., Rudowski R., Ware N. (1973) Lunar highlands composition: Apennine front. In *Proc. 4th Lunar Sci. Conf.*, Lunar Planet. Inst., Houstan, pp. 1445–1459.

Taylor S. R. (1982) *Planetary Science. A Lunar Perspective*. Lunar and Planetary Institute, Houston.

Terada K., Anand M., Sokol A. K., Bischoff A. and Sano Y. (2007) Cryptomare magmatism 4.35 Gyr ago recorded in lunar meteorite Kalahari 009. *Nature* **450**, 849–853.

Thompson, Jr., J. B. (1982) Composition space. An algebraic and Geometric approach. In *Characterization of Metamorphism Through Mineral Equilibria* (ed. J. M. Ferry). Mineralogical Society of America, Washington, DC, pp. 1–31.

Turner G. (1971) ^{40}Ar–^{39}Ar dating: the optimization of irradiation parameters. *Earth Planet. Sci. Lett.* **10**, 227–234.

Walker D., Longhi J. and Hays J. F. (1976) Heterogeneity in titaniferous lunar basalts. *Earth Planet. Sci. Lett.* **30**, 27–36.

Warren P. H. and Kallemeyn G. W. (1993) Geochemical investigation of two lunar mare meteorites: Yamato-793169 and Asuka-881757. In *Proc. NIPR Symp. Antarct. Meteorites*, vol. **6.** Nat. Inst. Polar Res., Tokyo, pp. 35–57.

Wentworth S., Taylor G. J., Warner R. D. and Keil K. (1979) The unique nature of Apollo 17 VLT mare basalt. *Proc. 10th Lunar Sci. Conf.*, vol. 2. Lunar Planet. Inst., Houston, pp. 207–223.

Wiens R. C. and Pepin R. O. (1988) Laboratory shock experiments of noble gases, nitrogen, and carbon dioxide into basalt, and implications for trapped gases in shergottite EETA 79001. *Geochim. Cosmochim. Acta* **52**, 295–307.

Yanai K. and Kojima H. (1991) Varieties of lunar meteorites recovered from Antarctica. In *Proc. NIPR Symp. Antarct. Meteorites*, vol. **4.** Nat. Inst. Polar Res., Tokyo, pp. 70–90.

Yanai K., Kojima H. and Naraoka H. (1993) The Asuka-87 and Asuka-88 collections of Antarctic meteorites; Search, discoveries, initial processing, and preliminary identification and classification. In *Proc. NIPR Symp. Antarct. Meteorites*, vol. **6.** Nat. Inst. Polar Res., Tokyo, pp. 137–147.

Zeigler R. A., Korotev R. L., Jolliff B. L. and Haskin L. A. (2005) Petrography and geochemistry of the LaPaz Icefield basaltic lunar meteorite and source crater pairing with Northwest Africa 032. *Meteorit. Planet. Sci.* **40**, 1073–1101.

Associate editor: Christian Koeberl